
[All ETDs from UAB](#)

[UAB Theses & Dissertations](#)

2013

Intramural Electrical Uncoupling during Long-Duration Ventricular Fibrillation in Rabbit

Trenika A. Madden
University of Alabama at Birmingham

Follow this and additional works at: <https://digitalcommons.library.uab.edu/etd-collection>



Part of the [Engineering Commons](#)

Recommended Citation

Madden, Trenika A., "Intramural Electrical Uncoupling during Long-Duration Ventricular Fibrillation in Rabbit" (2013). *All ETDs from UAB*. 2362.

<https://digitalcommons.library.uab.edu/etd-collection/2362>

This content has been accepted for inclusion by an authorized administrator of the UAB Digital Commons, and is provided as a free open access item. All inquiries regarding this item or the UAB Digital Commons should be directed to the [UAB Libraries Office of Scholarly Communication](#).

INTRAMURAL ELECTRICAL UNCOUPLING DURING LONG DURATION
VENTRICULAR FIBRILLATION IN RABBIT

by

TRENIKA A. MADDEN

DR. STEVEN POGWIZD, COMMITTEE CHAIR

DR. XUN AI

DR. RAYMOND IDEKER

DR. ANDREW POLLARD

A THESIS

Submitted to the graduate faculty of The University of Alabama at Birmingham,
in partial fulfillment of the requirements for the degree of
Master of Science in Biomedical Engineering

BIRMINGHAM, ALABAMA

2013

Copyright by
Trenika A. Madden
2013

INTRAMURAL ELECTRICAL UNCOUPLING DURING LONG DURATION VENTRICULAR FIBRILLATION IN RABBIT

TRENIKA A. MADDEN

BIOMEDICAL ENGINEERING

ABSTRACT

Ventricular fibrillation is a lethal cardiac arrhythmia which alters electrophysiological properties of the myocardium while concurrently inducing global ischemia and is associated with high mortality rates. Studies on the organization of long-duration ventricular fibrillation (LDVF) have shown that an endocardial to epicardial (i.e. transmural) activation rate gradient exists during ventricular fibrillation in canine and human myocardium; however, the underlying mechanism is unknown. This study tested the hypothesis that the activation rate gradient reflects heterogeneous changes in tissue electrical resistivity resulting in differential transmural electrical uncoupling of the ventricular myocardium. LDVF (>5min) was electrically induced in anesthetized, open-chest rabbits using an AC stimulus. Intramural electrograms for activation mapping were recorded using bipolar plunge needle electrodes throughout the left and right ventricles. Intramural resistivity was measured in the sub-endocardial (Endo), midmyocardial (Mid), and sub-epicardial (Epi) layers of the basal anterior left ventricular wall using a novel, modified four-electrode resistivity technique. Activation mapping and resistivity were assessed concurrently in each study. An activation rate gradient developed during LDVF in the left ventricle where the Epi developed a significantly slower activation rate compared to more endocardial levels of myocardium soon after fibrillation onset. This gradient occurred with spatiotemporal heterogeneity. LDVF induced immediate steep increases in Epi resistivity with Mid and then Endo increases developing subsequently.

Steep resistivity increase consistent with electrical uncoupling proceeded transmurally in the left ventricle with earliest rise developing in the Epi. The onset of Epi steep resistivity rise was closely associated with the development of the Endo-Epi activation rate gradient. Steep resistivity increases developed much more quickly during LDVF than during global myocardial ischemia. Our novel resistivity measurement system enabled us to observe a mechanism of ventricular fibrillation which had not previously been described. Steep resistivity increases indicating differential transmural electrical uncoupling occur with similar time course as the LDVF activation rate gradient and is most marked in the epicardium during early stages of ventricular fibrillation. Gap junction proteins such as Connexin43 may play a role. These findings suggest pharmacologic modulation of electrical coupling as a potential therapeutic approach to improve treatment for LDVF.

Keywords: electrophysiology, ventricular fibrillation, activation rate gradient, resistivity, electrical uncoupling

DEDICATION

I dedicate this work to my husband for his love, strength, and encouragement whether near or far and to my mother who is the best support system for which a daughter could ask.

ACKNOWLEDGEMENTS

I would like to thank the Department of Biomedical Engineering at the University of Alabama at Birmingham and my research advisor and chair of my committee, Dr. Steven Pogwizd, for his instruction, guidance, and advice throughout the duration of my graduate studies. I am grateful to the members of my thesis committee, which includes Dr. Xun Ai, Dr. Raymond Ideker, and Dr. Andrew Pollard, for their time as well as assistance and support toward this research.

I express my sincere gratitude to the research staff in the Cardiac Rhythm Management Laboratory, including Sharon Melnick, Dennis Rollins, Shannon Salter, Frank Vance, and Cheryl Killingsworth, who has played a very instrumental role in the completion of research experiments necessary to this project. A special mention must be made of Sharon who provided countless hours of excellent surgical assistance during *in vivo* animal studies. I would also like to acknowledge Dennis for his assistance with the usage of mapping systems utilized for acquisition of data in this research project. Both Sharon and Dennis aided in the development and fabrication of the specialized resistivity array created specifically for this project. I am appreciative to Greg Hoeker and Ashleigh Hood for lending their expertise in rabbit *in vitro* preparations and assistance with control *in vitro* resistivity experiments necessary for this project.

This research was supported by National Institutes of Health grant R01 HL080093.

TABLE OF CONTENTS

	<i>Page</i>
ABSTRACT	iii
DEDICATION	v
ACKNOWLEDGEMENTS	vi
LIST OF TABLES	ix
LIST OF FIGURES	x
LIST OF ABBREVIATIONS	xii
INTRODUCTION	1
Clinical Problem	1
VF Gradient	2
Electrical Uncoupling	4
Resistivity	5
Objectives	6
METHODS	9
Studies in the <i>in vivo</i> Rabbit Heart	9
Preliminary Studies in the <i>in vivo</i> Dog Heart	10
Control Studies of Global Ischemia in the Isolated Rabbit Heart.....	10
Activation Mapping System	12
Resistivity Measurement.....	13
Data Analysis	16
<i>Activation Mapping Analysis</i>	16
<i>Resistivity Measurement Analysis</i>	17
RESULTS	18
VF Induction	18
Activation Mapping	19
<i>Selection of Bipolar Mapping System</i>	19
<i>Preliminary Activation Mapping in Dog</i>	22
<i>Activation Mapping in Rabbit</i>	26
<i>Activation Selection Criteria</i>	27

<i>Activation Rate Gradient Develops During LDVF in Rabbit</i>	27
<i>Heterogeneous Development of ARG</i>	33
Resistivity	39
<i>Voltage Response Assessment for Resistivity Measurement</i>	39
<i>Voltage Response Selection Criteria</i>	39
<i>Stability of Electrode Array</i>	42
<i>Resistivity Measurement Does Not Alter VF Activation Rate</i>	44
<i>Characteristics of Transmural Changes in Intramural Resistivity</i>	44
<i>Changes Observed in Relative Resistivity</i>	46
<i>Relationship Between ARG and Resistivity in LDVF</i>	49
DISCUSSION	53
Discussion of Results	53
<i>VF Induction</i>	53
<i>Activation Rate Gradient</i>	54
<i>Resistivity</i>	57
Alternate Mechanisms for the Activation Rate Gradient.....	61
Future Direction	62
Limitations	63
Conclusion	66
REFERENCES	67
APPENDIX: IACUC Approval Form	72

LIST OF TABLES

<i>Table</i>	<i>Page</i>
1 LDVF Duration Following 60s AC in Rabbit.....	19
2 Transmural LV Average AR During LDVF.....	31
3 Activation Rate Gradients Observed in LV Sites During LDVF	34
4 Onset Time of Steep Resistivity Rise	47
5 Epicardial Steep Resistivity Rise Onset vs. Activation Rate Gradient Onset.....	52

LIST OF FIGURES

<i>Figure</i>	<i>Page</i>
1 LV Activation Mapping Needle.....	12
2 Activation Mapping and Resistivity Measurement Equipment Diagram.....	12
3 Four-electrode Resistivity Array.....	13
4 Four-needle Resistivity Array.....	14
5 VF Duration Following AC Stimulation	18
6 Preliminary Unipolar Electrogram Analysis.....	20
7 Preliminary Unipolar and Bipolar Electrogram Analysis.....	21
8 Activation Rate Gradient Development in Dog.....	23
9 Time of Gradient Onset in Dog by Location	24
10 Heterogeneous Gradient Development in Dog.....	25
11 Four-needle Resistivity Array in the <i>in vivo</i> Rabbit Heart	26
12 Rapid Rabbit Cycle Lengths During LDVF	28
13 Activation Rate Gradient Development in Rabbit.....	29
14 Time of Gradient Onset in Rabbit by Location	32
15 Heterogeneous Gradient Development in Rabbit.....	33
16 ARG Development by Ventricular Location	35
17 Inactivity Amid Areas of Activity During LDVF in Rabbit.....	36
18 ARG Does Not Develop Due to an Endo Threshold AR.....	37
19 Endo Cycle Length For Conducted vs. Non-Conducted Activations.....	38

20	HPF and Exclusion Criteria for Resistivity Analysis	41
21	Attenuation of Unfiltered Data Resulting from HPF	42
22	Voltage Response Pulse Diagram.....	42
23	Stability of Resistivity Electrode Array During SR.....	43
24	Average Resistivity Values During SR in Rabbit.....	43
25	Rabbit LDVF Activation Rates With and Without Resistivity Measurement.....	44
26	Representative Rabbit Intramural Relative Resistivity During LDVF	45
27	Mean Intramural Relative Resistivity During LDVF in Rabbit.....	48
28	Relative Resistivity During LDVF vs. Global Ischemia in Rabbit.....	49
29	Intramural AR vs. Intramural Resistivity During LDVF in Rabbit	51

LIST OF ABBREVIATIONS

AC	Alternating current
AR	Activation rate
ARG	Activation rate gradient
Cx43	Connexin43
d	Interelectrode distance
DC	Direct current
ECG	Electrocardiogram
Endo	Sub-endocardium
Epi	Sub-epicardium
ETCO ₂	End-tidal carbon dioxide
HPF	High pass filter
I	Current
λ	Constant of resistivity
LAD	Left Anterior Descending (coronary artery)
LDVF	Long-duration ventricular fibrillation
LV	Left ventricle
Mid	Mid-myocardium
ρ	Resistivity
RV	Right ventricle
σ	Standard deviation

SCA	Sudden Cardiac Arrest
SpO ₂	Saturation of peripheral oxygen
SR	Sinus rhythm
V	Potential difference
VF	Ventricular fibrillation

INTRODUCTION

Clinical Problem

Sudden cardiac arrest (SCA) is often a lethal outcome of cardiac disease in which an electrical disorder causes abrupt cessation of cardiac pumping. SCA leads to approximately 450,000 deaths each year in the U.S. alone.¹ Ventricular fibrillation (VF) is a major cause of SCA. During this lethal cardiac arrhythmia, erratic electrical activations cause rapid but uncoordinated contraction of cardiac fibers resulting in ineffective contraction of the heart and consequently loss of cardiac output. VF alters electrophysiological properties of the myocardium while concurrently inducing global ischemia. The current intervention for VF is defibrillation to electrically reset the heart. The chance of successful defibrillation leading to patient survival decreases by 7% to 10% per minute of VF.² Often, out-of-hospital VF is not defibrillated until 8 to 12 minutes of VF,³ which is long-duration VF (LDVF). While the out of hospital survival is low in these settings, successful resuscitation with neurological and cardiovascular recovery is possible and has been obtained.⁴ The myocardial properties which determine successful therapy and survival are largely unknown, but are likely related to the mechanisms which sustain LDVF.

The pattern of activation during ventricular fibrillation is thought to be maintained by reentrant mechanisms originating from a mother rotor⁵ or multiple reentrant circuits.⁶ Reentry occurs when the end of an activation wavefront path connects to its origin, activation proceeds continuously, and conduction velocity remains similar from the path end to re-initiation of the activation wavefront.⁷ During VF, complex activation

sequences are thought to occur when wavefronts encounter an area of refractory tissue causing wavebreak.^{8,9} Decreased conduction velocity increases total activation time which eventually exceeds the coupling interval resulting in areas of functional block.^{7,10}

VF Gradient

Several studies on the organization of LDVF have shown that a transmural gradient of activation rate (AR) exists in the canine^{11,12,13} and human¹⁴ myocardium. As VF progresses, coupling interval regularity and discreteness of activation deflections decreases first at the epicardium and progresses transmurally toward the endocardium.

Worley et al. demonstrated in a canine bipolar plunge electrode study that an LV endocardial to LV epicardial (transmural) activation rate gradient develops as soon as 2 minutes after onset of electrically induced ventricular fibrillation.¹³ Distinctness of electrogram deflections decreased as a function of distance from the endocardium and time where epicardial levels first showed decreased distinctness. The regularity of the R-R interval decreased and the average R-R interval increased first in the epicardial levels and progressively toward the endocardium. The activation rate gradient did not occur when animals were maintained on cardiopulmonary bypass, but developed shortly after bypass cessation. Their findings support the hypothesis that the gradient is due to effects of ischemia. They further show that the activation gradient is not a result of a gradient in temperature, high energy phosphate, or pH.

Cha et al. extended this study of activation rate gradient to test whether the development of the gradient in dog is due to cavitory blood sustaining the endocardium or Purkinje fiber resistance to ischemia.¹¹ Their results showed that in the absence of blood

in the RV cavity, an endocardial-epicardial activation rate gradient developed. This refutes the hypothesis that the gradient is due to preservation of the endocardium by oxygenated cavitory blood. Ablation of the right ventricular sub-endocardium resulted in slowing of both endocardial and epicardial activation rates over the course of VF and prevented development of the activation rate gradient supporting the notion that Purkinje fibers are the source for the sustained rapid endocardial rates. A study that compared septal activation rates to that in the endocardium and epicardium concluded that the activation rate gradient cannot be fully attributed to Purkinje fiber distribution.¹² They found sites of fastest activation located in the septum and at least 4mm away from an endocardial surface containing the Purkinje layer. Additionally, septal mid-myocardial and epicardial activation rates were similar to LV endocardial rates and consistently faster than surrounding RV and LV epicardial rates. While these studies have successfully refuted several hypothesis of the activation rate gradient, the mechanism for the decreased conduction and reduced excitability that develops during LDVF has yet to be described.

Optical mapping experiments^{15,16} in the isolated rabbit heart presented findings that the dominant frequency of the ECG slows significantly during non-perfused VF. Perfusion prevents rate slowing and the ECG remains rapid and highly irregular. Also, reperfusion restores rates to that comparable to control (perfused) conditions. Epicardial electrode mapping studies¹⁷ in isolated rabbit hearts have shown similar results. These findings indicate that the slowing induced by VF that occurs in hearts *in vivo* is an effect of fibrillation-induced ischemia.

Significant epicardial VF activation rate differences develop between the left and right ventricle in isolated rabbit hearts during ischemia where LV epicardial rates become slower than RV epicardial rates.^{15,18} Meanwhile, LV endocardial rates remain similar to RV endocardium. A difference in activation rate develops between LV endocardium and LV epicardium¹⁸ similar to that shown in dog. The limitations of these studies in rabbit are two-fold. First, these studies have only investigated VF in the isolated heart. These studies are unable to fully describe the natural progression of VF that occurs in the intact heart. Secondly, there have been no studies to investigate activation rates transmurally. Most studies have only measured activations on the epicardium.^{15,16,17} Wu et al investigated the activation rate of the endocardium and epicardium; however, separate methods and systems were used to measure each of these layers. Information about how the activation rate gradient progresses transmurally has yet to be investigated in the rabbit heart.

In an investigation of VF in myopathic human hearts, Massé et al. found an endocardial to epicardial gradient develops within 3 minutes of VF with global ischemia.¹⁴ This study demonstrates the occurrence of a gradient phenomenon in human which also occurs in canine and rabbit hearts. Investigation of the gradient mechanism will yield information that may be translatable to the mechanism of VF in humans.

Electrical Uncoupling

We believe the gradient in activation rate may reflect heterogeneous biochemical changes in conduction. Cardiac conduction is mediated by gap junctions primarily composed of Connexin43 (Cx43), a phosphoprotein.¹⁹ These junctions serve as

intercellular electrical coupling channels permitting the rapid flow of ions during cellular excitation.^{20,21} Cells become uncoupled when gap junction resistance increases and Cx43 dephosphorylation occurs.²²

Resistivity

Electrical uncoupling can be observed by measuring changes in cardiac resistivity. Studies of myocardial ischemia have demonstrated that the steep increase in resistivity correlates with the onset of electrical uncoupling through the assessment of intracellular resistivity and Cx43 dephosphorylation.²²

Bridge, two-electrode, and four-electrode techniques have been used to measure biological electrical resistivity.^{23,24} Bridge techniques offer high resolution, however they are not the best fit for tracking resistivity in systems where rapid changes occur.²⁴ The two-electrode method uses two electrodes to both deliver current and measure resistivity.²³ However, the resistivity value obtained represents both the impedance of the tissue as well as the impedance at the electrode-tissue interface. Polarization can occur in the electrodes due to current delivery further complicating interpretation of the resistivity value. The four electrode method of measuring tissue resistivity (ρ) employs a set of four electrodes in a linear array and equally spaced, in which current (I) is delivered through the outer two electrodes and the resulting potential difference (V) is measured between the inner two electrodes.²⁵ For a homogenous, isotropic resistive medium the potential difference is defined²⁵ by Equation (1),

$$V = \rho I / 4\pi d \quad (1)$$

where d is the distance between the inner electrodes. However, this relationship only holds when electrode diameter can be considered negligible in comparison to interelectrode distance. In practice,^{25,26} the resistivity is calculated as in Equation (2),

$$\rho = V*d*\lambda / I \quad (2)$$

such that λ is a constant derived by delivering a current and measuring the potential difference in a solution of known resistivity (such as saline). Separate electrode pairs for current injection and voltage measurement can essentially eliminate the problem of electrode polarization.²⁴ Also, by measuring voltage with high input impedance, polarization can be averted. The four-electrode technique was chosen as the measurement system for this project. This technique was modified in order to perform intramural resistivity measurements for an assessment of transmural changes in coupling.

Objectives

Ventricular fibrillation alters electrophysiological properties of the myocardium while concurrently inducing global ischemia and is associated with high mortality rates. Studies on the organization of long-duration ventricular fibrillation have shown that a transmural gradient in activation rate exists during ventricular fibrillation in canine and human myocardium. The mechanism causing this rate gradient is currently unknown, but may result from electrical uncoupling of the ventricular myocardium. Investigation of the course of electrical uncoupling during long-duration ventricular fibrillation is clinically

relevant in that it may yield new information about the mechanism of the LDVF activation rate gradient.

Hypothesis: The LDVF activation rate gradient reflects heterogeneous changes in cardiac conduction resulting in differential transmural electrical uncoupling of ventricular myocardium.

Specifically, significant changes in myocardial resistivity reflecting electrical uncoupling occurs transmurally beginning in the epicardium and proceeding transmurally toward the endocardium.

The first objective is to develop a model of LDVF in the *in vivo* rabbit heart. Few if any studies on the activation rate in rabbit have been performed *in vivo*. This type of model would allow for investigation of VF in the intact, innervated rabbit myocardium.

The second objective is to perform transmural activation mapping LDVF in anesthetized, open-chest rabbits and describe the development of the activation rate gradient in this species. Description of the activation rate gradient development using transmural activation mapping in the *in vivo* rabbit heart is a novel concept in itself. No studies to our knowledge have performed VF mapping in the sub-endocardial (Endo), mid-myocardial (Mid), and sub-epicardial (Epi) layers of the rabbit left ventricle concurrently to describe the progression of the activation rate gradient. Investigation of the activation rate gradient using bipolar plunge needle mapping electrodes will yield new information about LDVF in this species.

The third objective is to develop and utilize a method of multi-level intramural resistivity measurement. Information beyond single level resistivity measurement during regional or global ischemia has not previously been obtained. Furthermore, no studies

have assessed resistivity during VF. The use of a multi-level intramural resistivity measurement method will yield novel data to indicate the progression of transmural electrical uncoupling during LDVF in any species. A modified four-electrode resistivity technique developed using plunge needles will be used for intramural resistivity measurements in the sub-endocardial, mid-myocardial, and sub-epicardial layers of the basal anterior left ventricle to assess transmural changes in resistivity. Resistivity will be measured concurrently with activation mapping during LDVF.

The fourth objective is to correlate the development of the activation rate gradient with transmural changes in resistivity. Comparison of the time course of the activation rate gradient with the time course of transmural resistivity steep increases will determine whether a relationship exists between these two parameters and subsequently whether electrical uncoupling is the mechanism by which the activation rate gradient develops.

METHODS

Studies in the *in vivo* Rabbit Heart

Seven adult New Zealand White rabbits of either sex (weighing 2.99-3.69kg) were anesthetized with 45mg/kg of ketamine. The rabbits were intubated with an endotracheal tube and anesthesia was maintained with 2-3% isoflurane in oxygen. After the base of the tail, the chest, and the neck were shaved, a 22 gauge intravenous catheter was placed in the marginal ear vein and flushed. The rabbits were transferred from the preparation room to the operating room. Warm Lactated Ringers solution was delivered intravenously on a microdrip at 1 drop per 3 seconds. The rabbits were then instrumented for measurement of heart rate, blood pressure, SpO₂, ETCO₂, and temperature. The heart was exposed via midline sternotomy and suspended in a pericardial cradle. The chest cavity was covered with a thin, flexible plastic to retain heat and moisture and occasionally moistened with warm saline. Body core temperature was controlled through the use of heating pads to maintain temperature within a narrow range.

For each study 14 to 17 bipolar plunge needles (88-106 transmural sites, see **Activation Mapping System** for further description) were placed in the LV and sewn in the RV for transmural activation mapping. RV needles were sewn in to reduce the chance of electrode dislodgement from the thin RV wall. The distance between needles within each ventricle was approximately 0.6-2cm. A four-needle resistivity array was inserted into the basal anterior LV parallel to the LAD for resistivity measurement (see **Resistivity Measurement** for further description). Two stainless steel wires were sewn onto the anterior RV epicardium 1cm apart for AC current delivery. After insertion of all

needles, 60 minutes of normal sinus rhythm was observed to allow stabilization and reduction of the injury current. Baseline measurements of activation mapping, resistivity, and ECG were recorded throughout the stabilization period. VF was induced with a 60s, 60Hz AC current (a duration necessary to obtain consistent VF induction, see **VF Induction**). Ventilation was terminated within 30 seconds of sustained VF. Resistivity measurements were successively recorded at the Endo, Mid, and Epi within 15-30s of VF induction and at each minute following for 30 minutes of VF. The first set of resistivity measurements were labeled as occurring at minute 1 of VF. Activation mapping was performed continuously for 30 minutes of VF. At completion of each study, needle locations were localized with labeled stainless steel pins; the heart was excised and preserved in 10% formalin.

Preliminary Studies in the *in vivo* Dog Heart

In a separate series of studies, activation mapping was performed in two female dogs weighing 9.2-9.4kg. Surgical preparations were done in a manner similar to that described for *in vivo* rabbit studies. After dogs were anesthetized with Telazol, the hearts were exposed, and 37-42 bipolar plunge needles were placed throughout the LV and RV. VF was induced with a 5-10s DC shock by touching a 9V battery to two electrodes sewn to the RV. Activation mapping was performed continuously for 30 minutes of VF.

Control Studies of Global Ischemia in the Isolated Rabbit Heart

Two male adult New Zealand White rabbits (weighing 3.6-3.9kg) received 2mL of heparin intravenously via the left ear vein, were sedated with an intramuscular

injection of 44 mg/kg of ketamine, and then anesthetized with 5% isoflurane via mask inhalation. After a surgical plane of anesthesia had been achieved, hearts were rapidly excised by thoracotomy. Hearts were transferred to a Langendorff apparatus and perfused through the aorta with Tyrode's solution at 37°C oxygenated with 95% O₂ and 5% CO₂ (in mM: 125.0 NaCl, 4.5 KCl, 24.0 NaHCO₃, 1.8 NaH₂PO₄, 0.5 MgCl₂, 5.5 Glucose, 1.8 CaCl₂, pH 7.4, in Milli-Q water with 100 mg/L albumin). Following cannulation, the perfusion flow rate was adjusted to maintain a retrograde perfusion pressure of 60-80mmHg. A four-needle resistivity array was inserted into the basal anterior LV for resistivity measurement. Three bipolar plunge needles were placed within 1 cm surrounding the resistivity array. Following electrode placement, hearts were transferred to a chamber and superfused in a bath of Tyrode's solution. All hearts were perfused continuously during electrode placement and a subsequent 30 minute stabilization period.

Baseline measurements of activation mapping, resistivity, and ECG were recorded throughout the stabilization period. Global ischemia was achieved through termination of perfusion for a 60 minute period. Resistivity measurements were successively recorded at the Endo, Mid, and Epi immediately following perfusion cessation and at every other minute following for 60 minutes of ischemia. The first set of resistivity measurements were labeled as occurring at minute 0. Activation mapping was performed concurrently with resistivity measurement. At completion of each study, needle locations were localized with labeled stainless steel pins and the heart was preserved in 10% formalin.

Activation Mapping System

Bipolar plunge needle electrodes previously designed in the UAB Cardiac Rhythm Management laboratory were used for transmural activation mapping. All needles contained 76 μ m diameter silver wire electrodes with a 0.5mm interelectrode distance. The most epicardial needle was approximately 0.5mm from the needle bend. LV plunge needles (Figure 1) contained 9 electrodes (8 bipolar pairs) and RV plunge needles contained 3 electrodes (2 bipolar pairs).

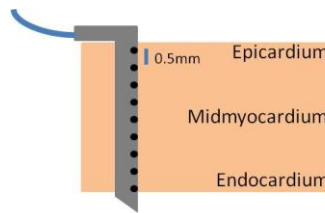


Figure 1: Schematic of an electrode used for activation mapping in the rabbit left ventricle. The needle (gray area) houses 9 electrodes exposed through epoxy and represented by the black circles. (Figure not drawn to scale.)

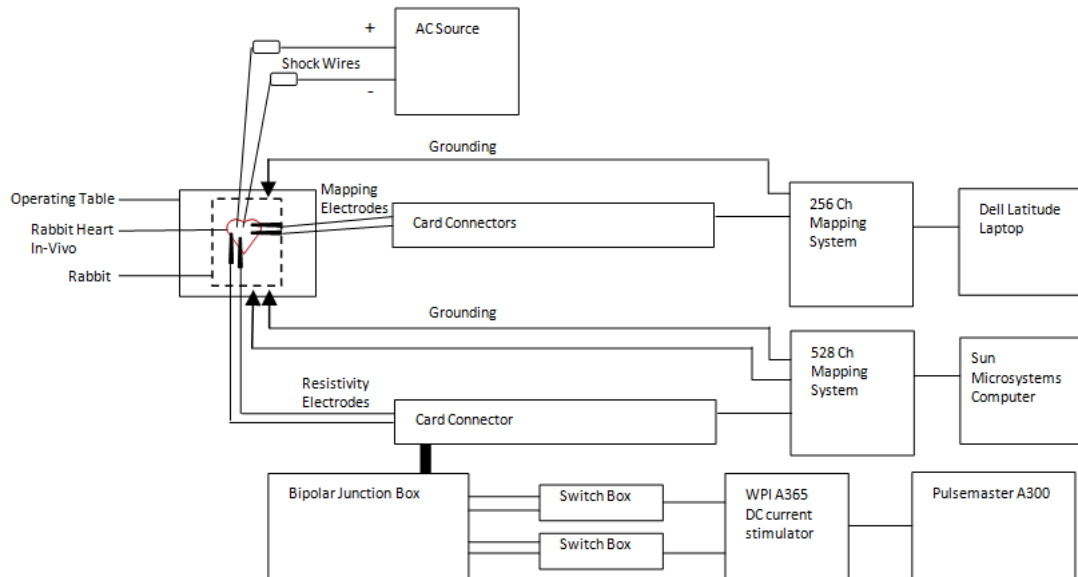


Figure 2: Diagram of mapping and stimulation equipment used for activation mapping and resistivity measurement during LDVF.

All plunge needles were connected to a 256-channel mapping system (Figure 2) and a ground electrode was placed at the left leg. Signals from plunge needles and limb

leads I, II, and III were sampled at 1 kHz and bandpass filtered from 40 to 500Hz. The data was saved to file and analyzed off-line.

Resistivity Measurement

Myocardial resistivity was measured using a four electrode resistivity technique to employ a set of four electrodes equally spaced in a linear array, in which current (I) was delivered through the outer two electrodes and the resulting potential difference (V) was measured between the inner two electrodes (Figure 3). We designed plunge needle electrodes (Figure 4) to measure resistivity in multiple levels of the tissue including the sub-endocardium, mid-myocardium, and sub-epicardium. In summary, plunge needles contained five 0.28mm diameter silver wire electrodes with a distance of 2mm between electrodes along the needle. The most epicardial electrode was approximately 1mm from the needle bend. The four plunge needles were inserted into the LV parallel to the LAD with a linear spacing of approximately 2.5mm (a spacing widely used for resistivity measurements).^{27,28,29,30,31}

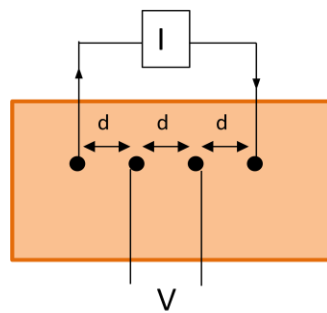


Figure 3: Diagram of a four-electrode array used to measure resistivity. The four electrodes are represented by black circles with an interelectrode spacing of distance d . Current delivery is represented by the lines and arrows connected to current, I , flowing through the outer two electrodes. Voltage, V , is measured using the inner two electrodes.

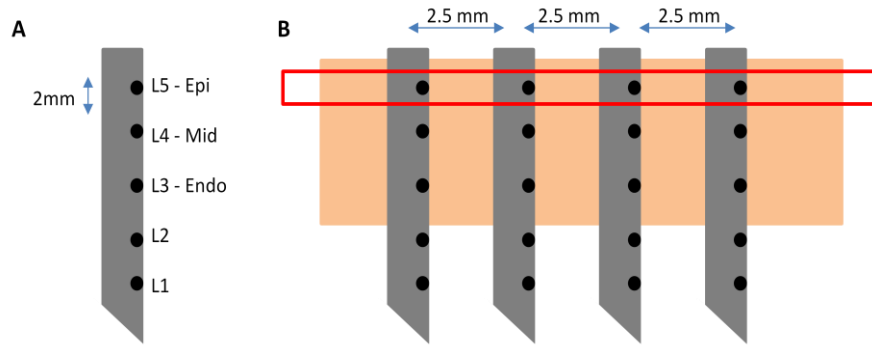


Figure 4: Schematic of a plunge needle used for resistivity measurement (A) and the four needle array used to measure intramural resistivity for several layers (B). Each plunge needle contains 5 electrode which are referred to by level along the needle: L1 (level 1), L2 (level 2), L3 (level 3), L4 (level 4), and L5 (level 5). For all rabbit studies, L5 was always the most epicardial electrode and referred to as the Epi level electrode and L3 was the most endocardial electrode and referred to as the Endo level electrode. The red rectangle (B) indicates a four electrode array composed of one electrode from the same level in each needle that is used to make an intramural measurement of a layer of the myocardium. (Drawings are not to scale.)

The plunge needle electrodes were fabricated according to methods commonly used in the Cardiac Rhythm Management Laboratory. Heat shrink tubing (3M FP301 3/64") approximately 4cm in length was used as a mold to create the body of the needle for the plunge needle electrodes. A milling machine was used to pierce 5 holes into the heat shrink tubing with a spacing of 2mm for electrode locations. Two strands of fiberglass were threaded through the hollow tubing. Since electrodes used for resistivity measurement in cardiac tissue range 0.2-0.4mm in diameter,^{26,27,29,30,31,32} 0.28mm diameter silver wire was selected due to its compliance within this range and availability in the lab. A silver wire was threaded through each of the five tubing holes until only 1cm of wire protruded through the electrode hole creating an electrode unit. The loose wires at the opposite end of the unit were braided. The heat shrink tubing was carefully shrunk around the wires using a butane torch. The electrode unit was placed on an aluminum right angle mold with the most proximal electrode (to later be designated most epicardial electrode) 1mm from the mold bend. After heating the tubing at this proximal end, the unit was bent into a right angle. Epoxy was injected into the distal and proximal ends of

the tubing to fill in epoxy around the wires. After the epoxy was cured at room temperature for 30 minutes, the unit was placed in an oven to bake at 80°C for 1 hour, and allowed to cure an additional 12 or more hours at room temperature. The heat shrink tubing was then removed from the electrode unit. The wires were trimmed with a #11 scalpel to expose the silver at the needle surface. The needle point was created by using the scalpel to cut the end of the epoxy into an approximate 45° angle; the point was smoothed and refined with an emory cloth. Insulation was removed from the ends of the braided wires, each end was soldered to a pin connector, and then all five pins were placed in a plastic connection card. Four plunge needles were created using these fabrication methods.

Resistivity within three intramural levels was measured using different levels of electrode groups (e.g. The subepicardial resistivity was determined by injecting current into the most epicardial electrodes of the outer two needles and measuring current between the most epicardial electrodes of the inner two needles.) A subthreshold direct current consisting of rectangular pulses of alternating polarity³³ ($\pm 10\mu\text{A}$, 10ms pulse width, 200ms delay) was delivered across the outer electrodes and potential difference was measured between the inner electrodes. The tissue was probed for 10s within each level with 5s separating each measurement. All plunge needles were connected to a 528-channel mapping system (Sun Microsystems) with a high-input impedance, sampled at 2 kHz and bandpass filtered from 0.5 to 500Hz.^{34,35} The data was saved to file and analyzed off-line.

Data Analysis

Activation Mapping Analysis

I developed a set of automated algorithms in Matlab 7.10 to determine activation times in bipolar electrograms from each electrode during sinus rhythm (SR) and VF. This algorithm selected activations using a 35ms search window to find rapid deflections with maximum magnitude greater than an absolute value of 0.25mV. The search window progressed forward 35ms after each selected activation to continue the search. Electrotonic deflections were excluded if the deflection was less than 50ms from an activation and: 1) the magnitude of the deflection was less than 50% that of the nearest activation, or 2) the slope of the deflection was less than 33% that of the nearest activation. Double potentials were labeled as deflections without an isoelectric period¹¹ of at least 3 time samples (3ms) separating them. If double potentials were identified, only the deflection with the greatest absolute magnitude was called as an activation. For all activations, the time of greatest absolute magnitude greater than 0.25mV was chosen as the activation time.⁷ Automated analysis was followed with manual analysis reviewing to confirm accurate activation selection. Average activation rate was calculated as the average number of activations per second over a 3s time interval. Averages were calculated immediately after VF induction and within 5s of each resistivity measurement set at minutes 1-20 after VF induction. The first VF analysis time point is considered as minute 1 of VF. Areas with no activations were considered to have an activation rate of 0Hz. SR was also analyzed using the same methods. Activation rate differences between electrograms on the same needles at each time point were tested using Student's t-test ($p=0.05$). Activation rate gradient was defined as the time when the first of at least 3

consecutive occurrences of significant difference in the activation rate was observed between the most endocardial and most epicardial point along the same needle. Average activation rate gradient was defined as the time when the first of at least 3 consecutive occurrences of significant difference was observed between the average of activation rates of all epicardial sites compared to all endocardial sites. Data from any electrode showing poor signal quality, unstable baseline, or low voltage ($<0.25\text{mV}$) during normal sinus rhythm or initial VF measurement were excluded from analysis.

Resistivity Measurement Analysis

I also developed an algorithm in Matlab 7.10 for analysis of bipolar voltage response data. This algorithm measures the magnitude of every voltage response over a 10s segment of data for each minute of VF and also for SR. The magnitudes of all positive voltage response pulses (with exceptions, see ***Voltage Response Selection Criteria***) were averaged for each time segment analyzed. Resistivity (ρ) was calculated by Equation (2) where V is the average voltage response, d is distance between the inner electrodes, and λ is a constant derived prior to each experiment through calibration in 0.9% saline with known resistivity. Relative resistivity was calculated by dividing all resistivity values by the value of resistivity obtained just prior to VF or global ischemia induction.^{22,26,28,36} The onset of the steep rise in resistivity (indicating electrical uncoupling) was determined as the time when a 5% increase in relative resistivity from the previous measurement was observed and followed by a 3% increase.

RESULTS

VF Induction

VF induction was attempted using an AC current source. Current stimulation lasting less than 45s often resulted in short duration VF or failed VF induction (Figure 5). Current duration of 50-60s led to higher incidence of long-duration VF. Animals weighing 3.3-4.0kg most reliably developed long-duration VF exceeding 10 minutes when stimulated with 60s AC current. LDVF was more difficult to achieve in lighter animals (<3.3kg), even with 60s current.

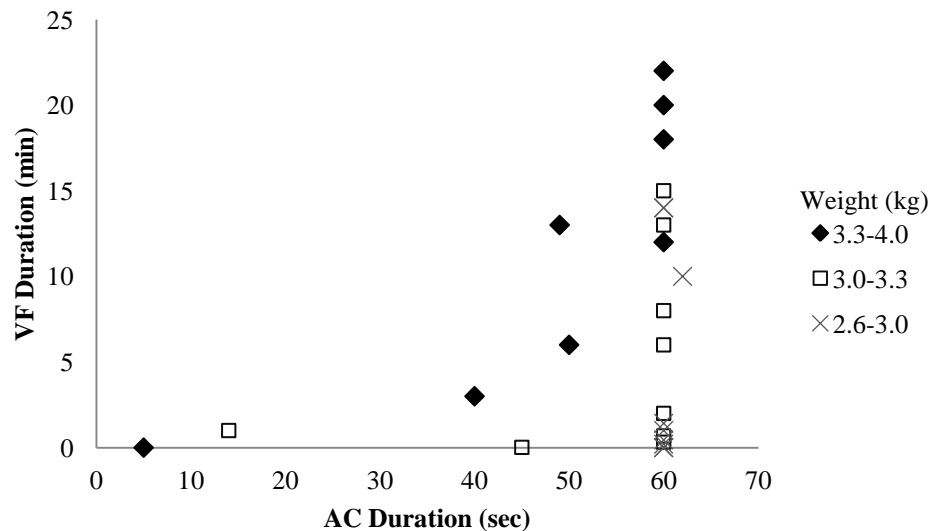


Figure 5: Duration of VF when using differing durations of AC current grouped by animal weight. Current durations less than 45s led to short-duration VF or no VF induction. Current duration of 60s resulted in VF episodes exceeding 10 minutes in heavier rabbits (3.3-4.0kg).

AC current stimulation lasting 60s was chosen as the method of VF induction for activation mapping and resistivity experiments. Duration of electrically induced VF (by 60s AC stimulus) is listed in Table 1 for each of the 7 rabbit studies in which activation mapping and myocardial resistivity measurement was performed. These studies included

animals which sustained VF a duration of 5 minutes or greater from a single VF induction attempt and which did not prematurely develop myocardial ischemia (assessed by epicardial cyanosis).

Study	Weight (kg)	VF Duration (min)
1	3.53	21
2	3.69	11
3	3.13	6
4	3.00	14
5	2.99	16
6	3.10	8
7	3.37	13

Activation Mapping

Selection of Bipolar Mapping System

Unipolar and bipolar mapping systems were available in the UAB Cardiac Rhythm Management Laboratory. When recording electrograms with a unipolar mapping system, analysis of the electrograms using a self-developed algorithm with minimum slope criterion ($dV/dt < -0.5mV$) often led to visually confirmed under-selection of activations (Figure 6A). Modification of this criterion to a lower threshold reduced under-selection in some electrograms and resulted in over-selection in others (Figure 6B). After off-line conversion of the unipolar electrograms to bipolar electrogram, analysis using a minimum magnitude based criterion resulted in more accurate selection of activations (Figure 7). Several iterations of a new Matlab algorithm which uses both magnitude and slope to identify activations in bipolar electrograms led to an automated process which requires much less manual analysis thereby reducing human bias. While both modes have

been used by other investigators to record cardiac electrograms in VF models, bipolar mapping using a bipolar mapping system was chosen for use in this study because of the higher accuracy of activation selection when automatically analyzing data with Matlab algorithms.

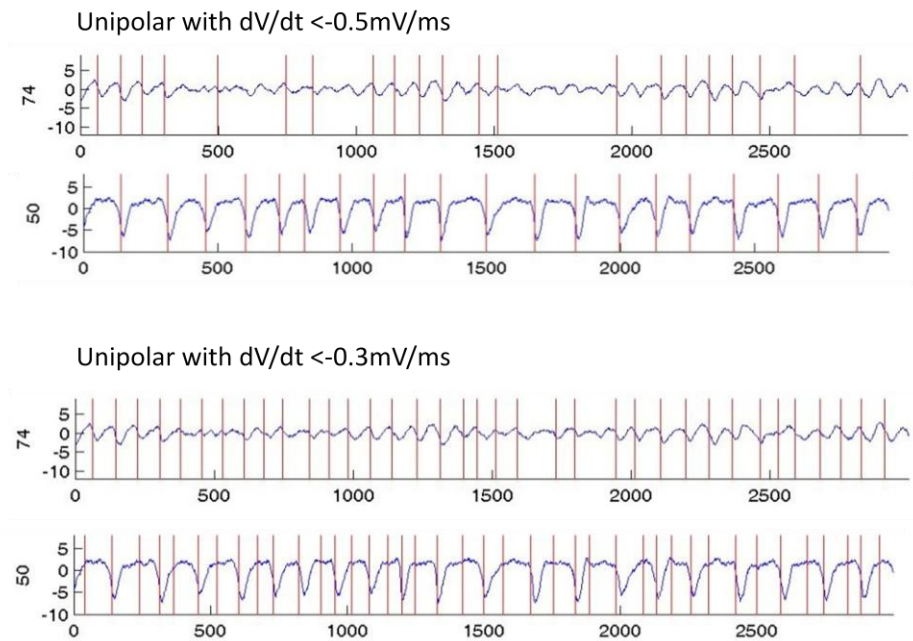


Figure 6: Representative unipolar electrograms that were analyzed using a slope threshold criterion of $dV/dt < -0.5\text{mV/ms}$ (A) and $dV/dt < -0.3\text{mV/ms}$ (B). In the top electrogram of (A), activations have been under-selected. However, after lowering the slope criterion and analyzing, the first electrogram is accurately selected, but the second electrogram is over-selected.

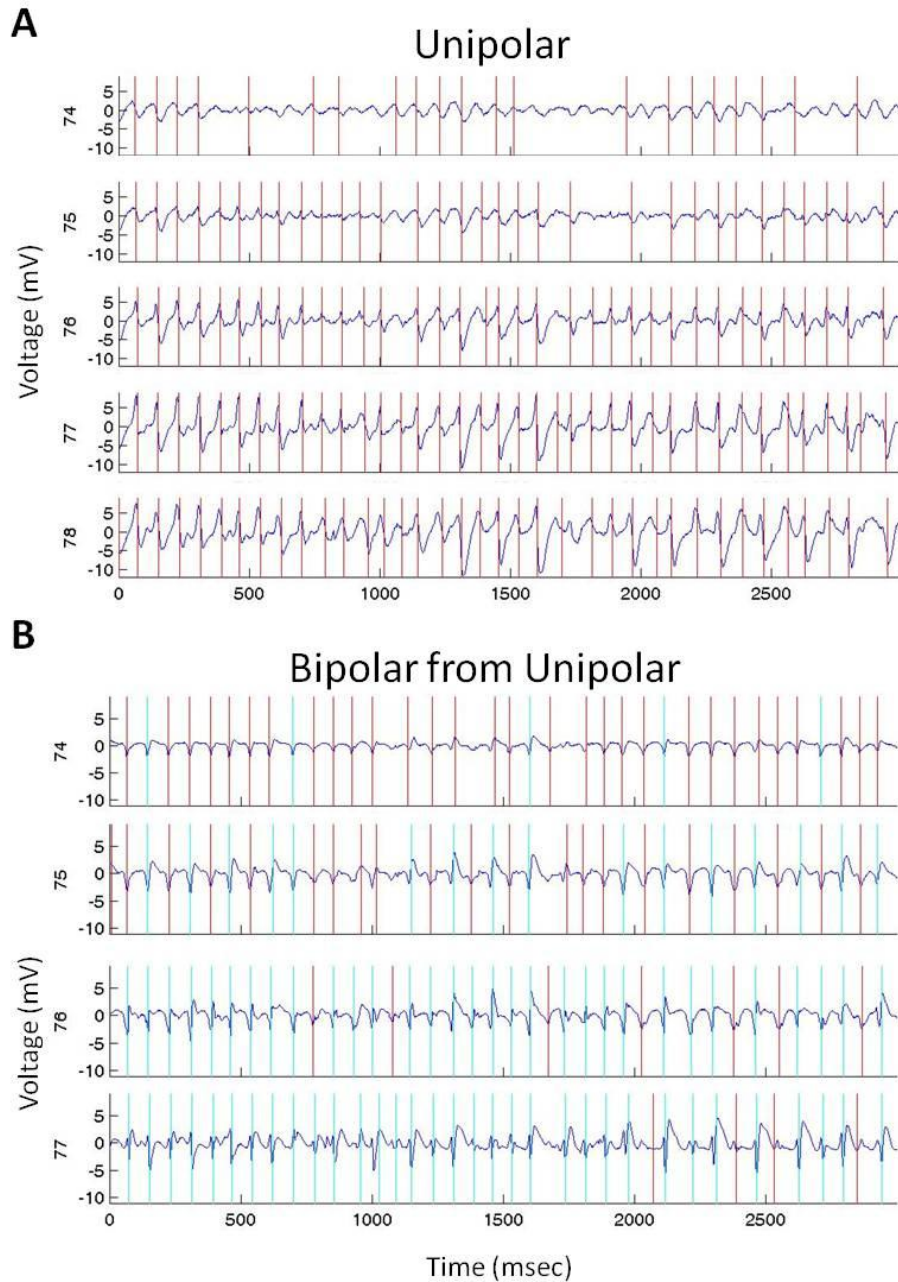


Figure 7: Transmural electrograms from one unipolar plunge needle plotted with red vertical lines indicating activations with slope at least $|0.4\text{mV/ms}|$ (A). Unipolar data converted to bipolar data and plotted with vertical lines indicating automatic activation selection as well (B). Blue lines on bipolar data indicate activations identified in first pass analysis which meet both criteria of being greater than $|0.25\text{mV}|$ and having slope greater than $|0.4\text{mV/ms}|$. Red lines indicate deflections identified in a second pass with magnitude greater than $|0.25\text{mV}|$. Analysis of unipolar electrograms resulted in under-selection of activations particularly in the first (most endocardial) line. Analysis of bipolar electrograms with a magnitude threshold of 0.25mV eliminates the under-selection.

Preliminary Activation Mapping in Dog

Bipolar activation mapping was performed in two dogs for the purpose of validating the activation mapping technique and comparison with data previously described by other investigators.^{11,12,13} During SR and 0-1 minutes of VF, activation rates were similar across all sites and layers mapped in the myocardium. Cycle lengths were regular and activation deflections were discrete. A significant difference in activation rate developed between the most endocardial point and the most epicardial point at several sites in the LV and RV as soon as 2 minutes of VF which agrees with previous findings.¹³ By 5 minutes of VF, a gradient was present at 78% (49 of 63) of sites across the two experiments. The development of the activation rate gradient in a representative site from one of the dogs of is shown in Figure 8. Activations are regular and discrete during normal sinus rhythm as well as at 1 minute of VF. At 5 minutes of VF, the AR in the Epi and the adjacent mid-myocardial layer is much longer than that of the more endocardial points. At 7 minutes, the AR has slowed dramatically in the Epi. The epicardium is completely inactive at that site by 10 minutes of VF when the Endo still shows activity. An activation rate gradient developed in 92% of LV sites and 60% of RV sites by 10 minutes of VF. We found that the onset of the activation rate gradient occurs heterogeneously across sites within the LV and RV. This has also been shown in dog previously.¹² As shown in Figure 9, in each dog the earliest sites of AR onset were often in the posterior LV. In other areas of the hearts, the time of onset was variable. This heterogeneity was very marked in some areas, such as that shown in Figure 10, where one site developed a gradient at 3 minutes and the adjacent site had not developed a gradient even after 10 minutes of VF.

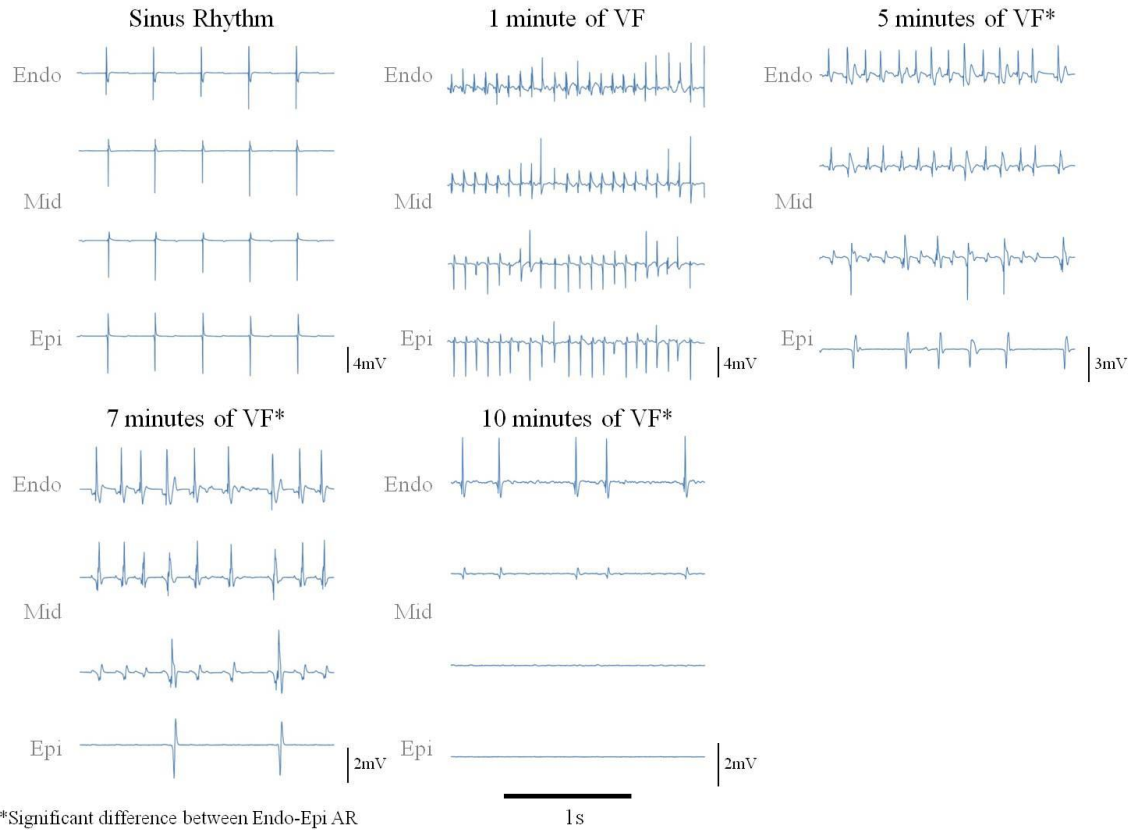


Figure 8: Bipolar electrograms from a plunge needle of a representative dog study during the first 10 minutes of LDVF. In each electrogram grouping (for each time point) the first plot is Endo electrogram, the next two plots are the successive Mid electrograms, and the fourth plot is the Epi electrogram. Activations are regular and discrete during normal SR as well as at 1 minute of VF. At 5 minutes of VF, the AR in the Epi and the adjacent Mid layer is much slower than that of the more endocardial points. At 7 minutes, the AR has slowed dramatically in the Epi. The Epi is completely inactive by 10 minutes of VF when the Endo still shows activity.

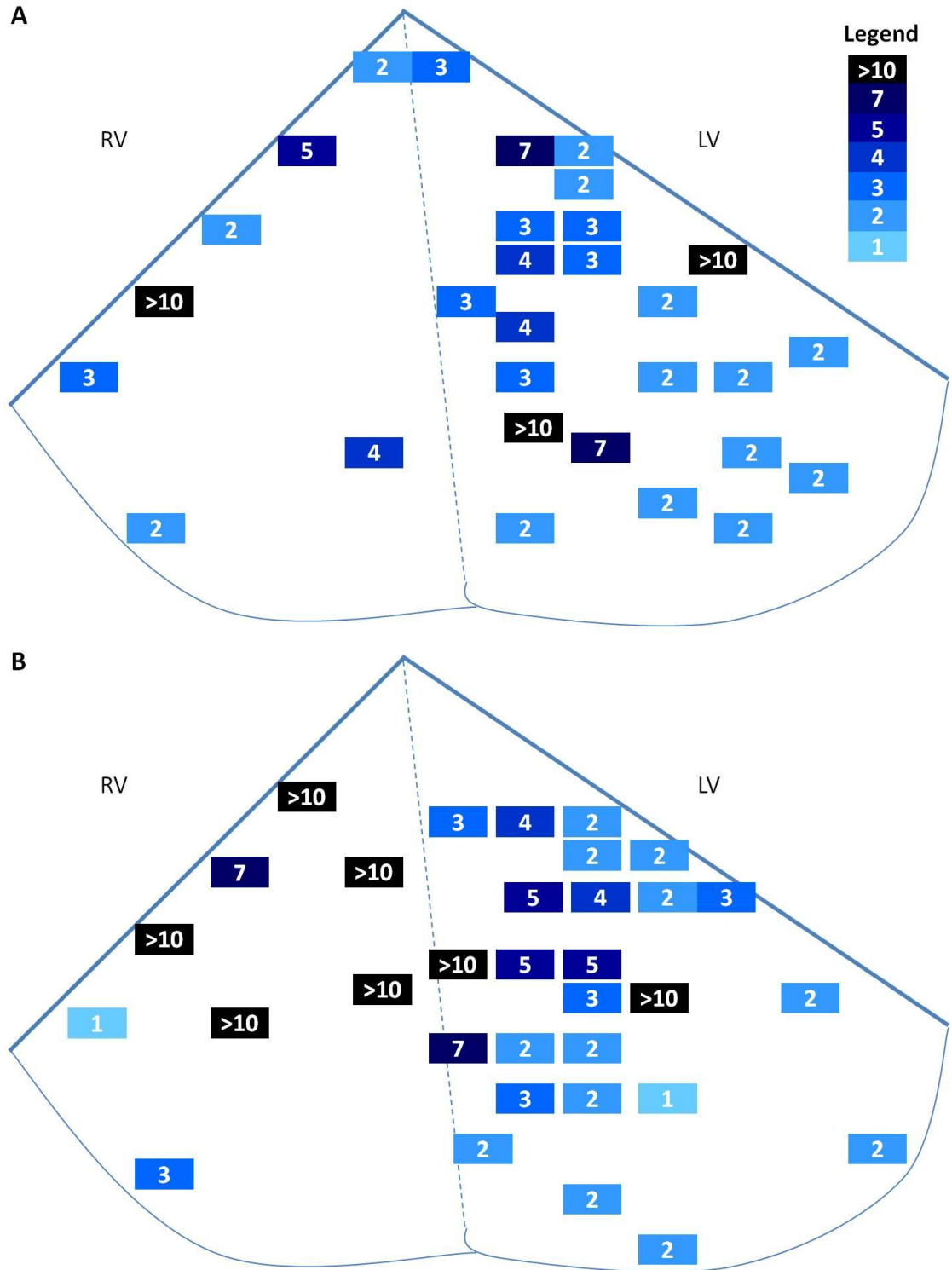


Figure 9: Heart diagram of the time of activation rate gradient onset during LDVF for each of two dogs studied. The color bar in the top right corner is a legend for the time in minutes of the onset of AR gradient. Activation rates were determined for up to 10 minutes of VF. Those sites marked with >10 indicate that no gradient was present at 10 minutes and either no gradient developed before inactivity occurred or a gradient developed but at a later time point.

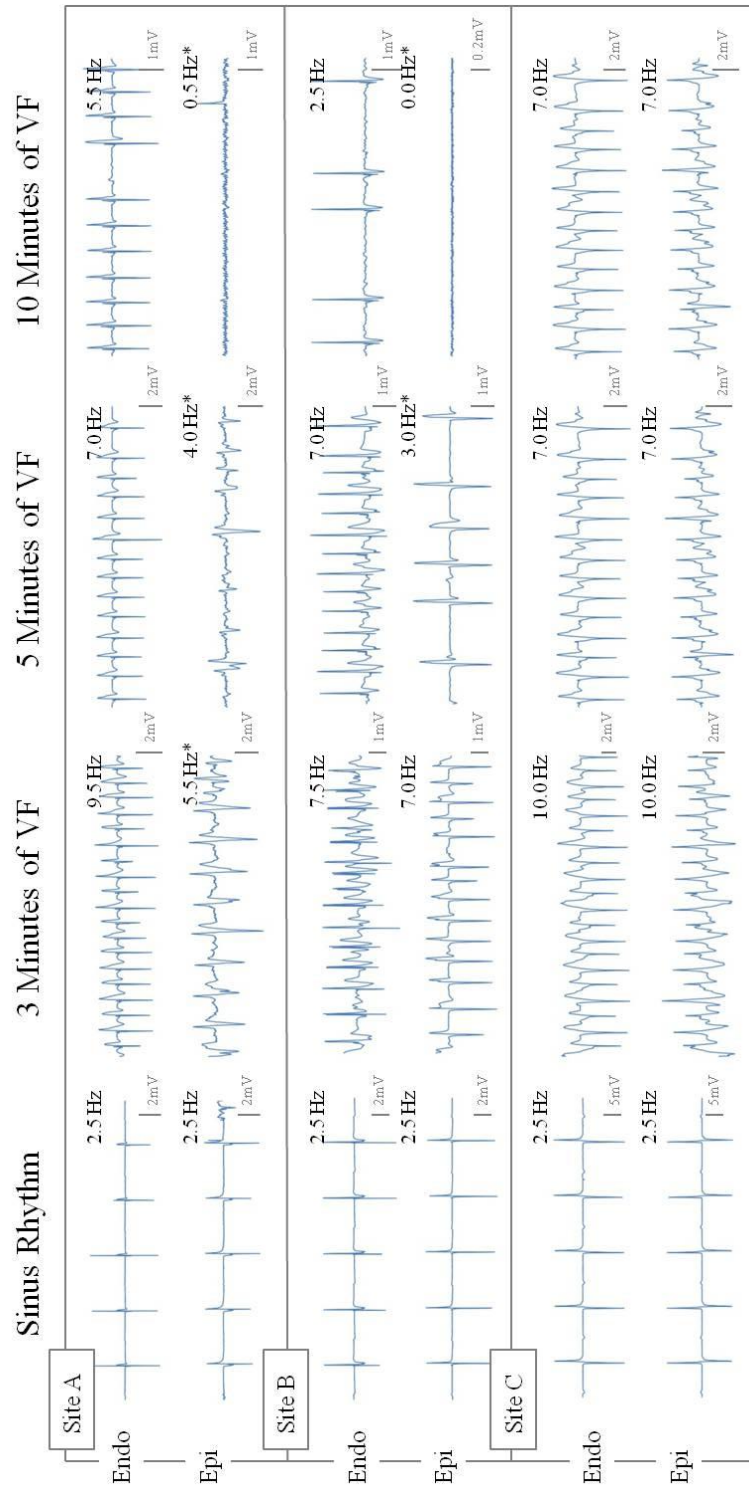


Figure 10: Electrograms from the most endocardial and most epicardial electrodes of three sites of one dog heart (heart map shown in Figure 9B) for selected time points up to 10 minutes of LDVF. At site A, a gradient develops at 3 minutes of LDVF and persists. At site B, CL are similar at SR and 3 minutes. A gradient does not develop until 7 minutes of LDVF. At site C, no gradient develops.

Activation Mapping in Rabbit

Rabbits were chosen as the focus for this research due to the many advantages that investigation in this species could bring. By mapping the rabbit heart, which is relatively small in size, higher electrode mapping density could be achieved. Transmural mapping of the rabbit ventricles *in vivo* could provide information which does not previously exist on transmural activation rates during LDVF in the rabbit heart. Furthermore, assessing LDVF in the normal, *in vivo* rabbit heart would allow parallel studies in the *in vitro* and heart failure models which have been developed in our laboratory.

Plunge needle electrode placement was a skill which was required in order to successfully perform transmural cardiac activation mapping. Fourteen to seventeen needles were placed in the *in vivo* heart (Figure 11) during normal sinus rhythm (212-300bpm). A suture was threaded through the apex to allow for gentle adjustment of the heart during placement and to make the posterior ventricular areas accessible. Care was taken to avoid puncture of major epicardial arteries to prevent the undesirable occurrence of myocardial ischemia.



Figure 11: Four needle resistivity array located in the anterior LV and surrounded by mapping needles in an *in vivo* rabbit heart.

Activation Selection Criteria

Activation rates during LDVF were initially measured using a minimum cycle length criterion of 50ms. Bipolar activation mapping data revealed activations with magnitude much greater than 0.25mV occurring with cycle lengths much less than this minimum and as short as 35ms. During these short cycle lengths, a clear return to baseline was observed between activations and there was little doubt that these deflections were true activations. To avoid underestimation of the true activation rate, the minimum cycle length was lowered to 35ms (Figure 12).

Activation Rate Gradient Develops During LDVF in Rabbit

From analysis of bipolar activation mapping electrograms, an LV endocardial to epicardial activation rate gradient (ARG) was also shown in the rabbit. In Figure 13, electrograms from the LV Endo, Mid, and Epi electrode from one needle in a representative rabbit show the development of the activation rate gradient during the course of LDVF. Activations occurred 1:1 from Endo to Epi during SR. At 1 minute of VF, the ARs were similar (10.5Hz, 10.5Hz, 10.5Hz in Endo, Mid, and Epi respectively). A significant difference in AR developed by 3 minutes where the Epi had a much slower rate than the Endo (15Hz vs. 10.0Hz respectively, $p < 0.05$). As VF progressed, the activations in the Epi developed increasingly irregular cycle lengths and rate continued to slow. Endo and Mid activation rates became more rapid during VF until after 5 minutes when the rate began to slow. But even by 10 minutes of VF, Endo activations were rapid (7.5Hz) and discrete.

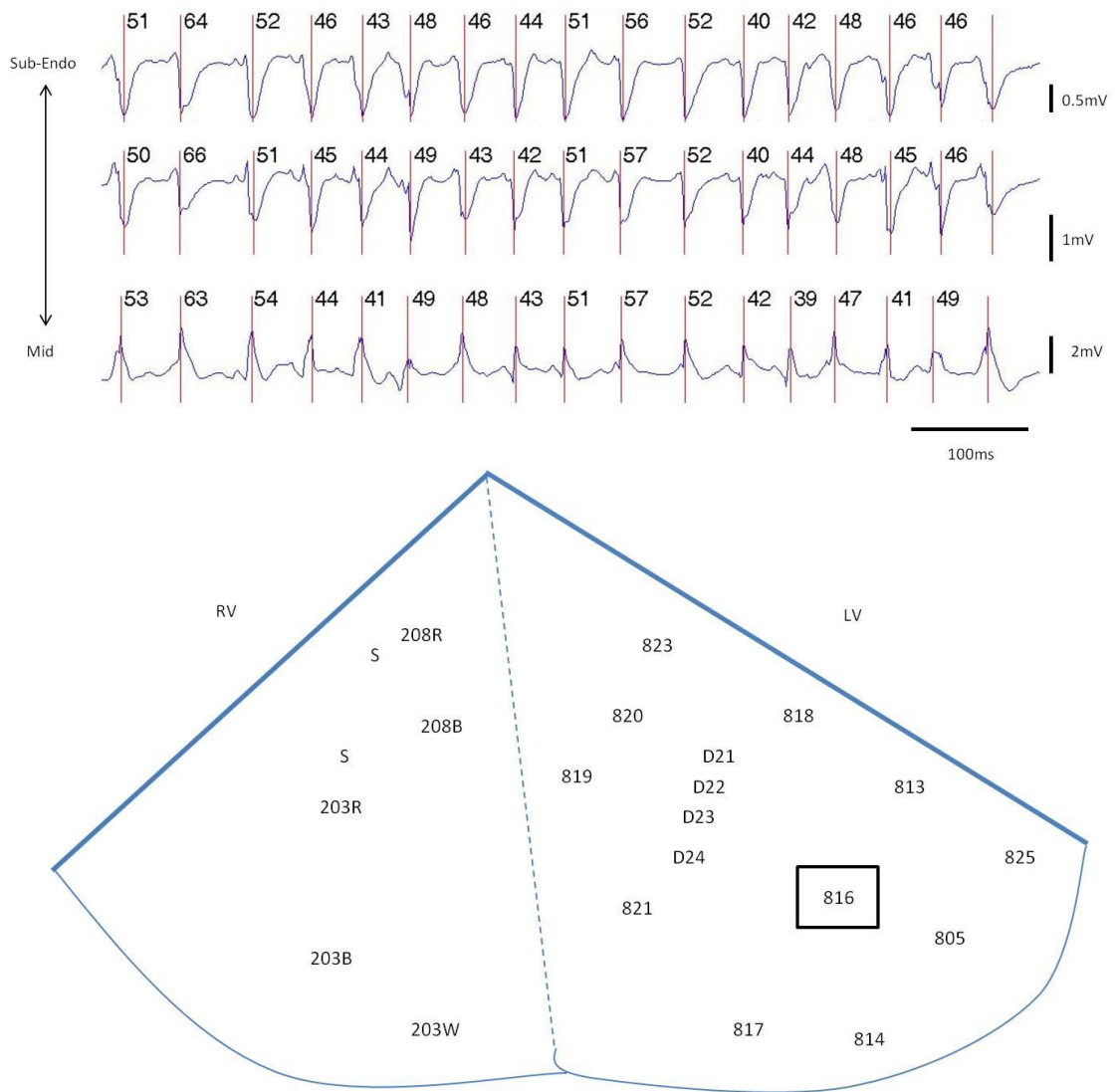


Figure 12: (Top) Electrograms recorded from 3 sites ranging sub-endo to mid at 1 plunge needle in the lateral LV (of a representative rabbit) are shown during 4 minutes of LDVF. Activations are marked with a vertical red line and cycle length is shown between each activation. Cycle lengths much shorter than 50ms are apparent in all 3 electrograms. (Bottom) A needle location map displays the location of all needles placed throughout the LV and RV. The representative electrograms (top) were obtained from the plunge needle labeled “816” located in the lateral LV and has been indicated with a black box.

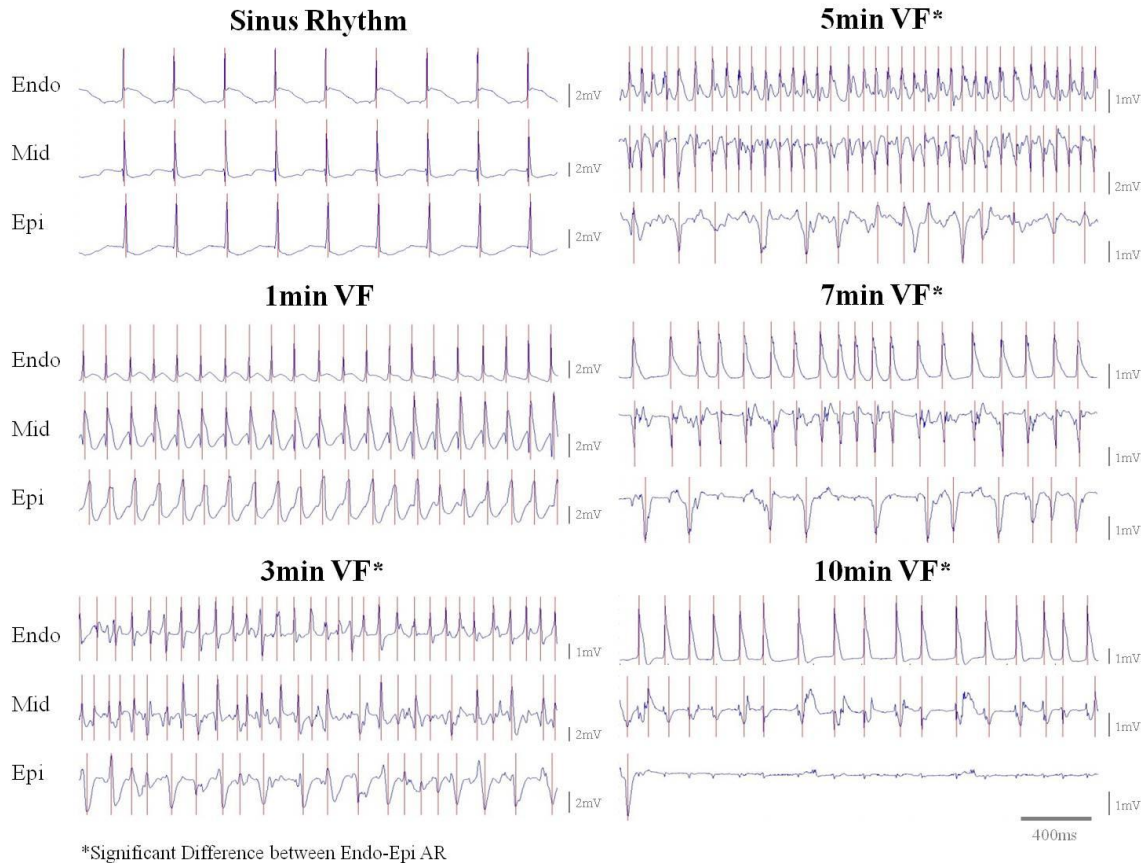


Figure 13: Electrograms from an Endo, Mid, and Epi site of 1 plunge needle in the LV (of a representative rabbit) are shown for several time points during LDVF. Activations are marked with a vertical red line. Activations occur 1:1 from Endo to Epi during Sinus Rhythm and 1min VF. A significant difference in AR develops as soon as 3min after VF onset where the Epi has a slower rate than the Endo. From 5 to 10min of VF, a dramatic slowing in rate is observed in the Epi while the Endo and Mid maintain activity.

LV Endo, Mid, and Epi average intramural activation rates for several time points during LDVF are shown for each study in Table 2. LV Endo had the most rapid rates throughout the course of VF. In each study, AR increased in the Endo and Mid from 1 minute to approximately 5 minutes of VF then began to decline. However, Mid AR did not increase to the same extent as the Endo with the exception of studies 6 and 7. In 4 of the 7 VF studies, maximal Epi rates occurred at by 1 minute of VF. A gradient in AR between the Endo and Epi developed within 2 minutes of VF for all studies ($p < 0.05$). This gradient persisted until the end of VF for all studies except study 4 which had very

irregular changes in VF rate after 5 minutes of VF. A significant difference in rate developed between the Endo and Mid within 2-3 minutes of VF for 5 studies ($p < 0.05$). For 4 of these studies (Studies 1-4) there was also a significant difference between Mid and Epi, in other words there was a significant difference in rate between each of the 3 layers. In the remaining study with an Endo-Mid gradient (Study 5), there was no significant difference in rate between Mid and Epi such that the Mid and Epi were similarly depressed in rate and both significantly slower than Endo. In Study 6, there was no significant difference between Endo and Mid, however both were significantly different from the Epi. Thus, the gradient was largely located between the Mid and Epi. In Study 7, there was no significant difference between Endo and Mid rate or Mid and Epi rates. There was 1 RV site for each of 4 studies in which an ARG developed during LDVF (Figure 14). This translates to only 20% of all mapped RV sites presenting a gradient, whereas 60% of RV sites developed a gradient in our dog studies. Each of these gradients developed in the rabbit apical anterior RV. The time of gradient onset ranged 3-8min. For all other sites, no gradient was present.

VF spontaneously terminated and converted to pulseless electrical activity with very slow activation rates within 6 or 8 minutes in 2 of 7 LDVF studies. For all other studies, VF persisted for 10 minutes or greater. This suggests that VF duration is related to maximal Endo AR achieved within the initial 5 minutes of VF. For the 2 spontaneously terminating VF episodes, maximal Endo AR averaged 13Hz, such that neither Endo AR ever exceeded 14Hz. In the remaining 5 studies which sustained VF 10 minutes or longer, maximal Endo AR averaged 16.4Hz, such that each Endo AR exceeded 14Hz. It may be necessary for some sites, particularly sites in the Endo, to

achieve very rapid rates greater than 14Hz for VF to last greater than 10 minutes. It is important to note that regardless of maximal Endo AR, an Endo-Epi ARG developed in all LDVF studies.

Table 2
Transmural LV Average AR During LDVF

Study	Layer	Activation Rate (Hz)							
		SR	1 min	2 min	3 min	5 min	10 min	15 min	20 min
1	Endo	4.3 ± 0.0	11.5 ± 0.4	15.0 ± 0.9	18.1 ± 1.4	18.3 ± 0.9	14.9 ± 2.4	8.8 ± 1.7	<i>0.0 ± 0.0</i>
	Mid	4.3 ± 0.0	10.5 ± 0.3	13.6 ± 0.5	14.5 ± 0.7*	14.6 ± 0.7*	9.5 ± 2.4	9.8 ± 1.5	<i>0.0 ± 0.0</i>
	Epi	4.3 ± 0.0	10.1 ± 0.4*	11.5 ± 0.6*	14.8 ± 1.1*	10.3 ± 1.4*	6.4 ± 1.9*	1.4 ± 1.1*	<i>0.0 ± 0.0</i>
2	Endo	4.3 ± 0.0	10.3 ± 0.1	12.1 ± 0.2	17.2 ± 0.8	16.4 ± 0.5	<i>6.6 ± 0.7</i>	<i>3.0 ± 0.3</i>	<i>2.7 ± 0.2</i>
	Mid	4.3 ± 0.0	10.2 ± 0.2	11.0 ± 0.3*	12.2 ± 0.8*	11.0 ± 0.9*	<i>6.8 ± 0.5</i>	<i>3.7 ± 0.6</i>	<i>1.5 ± 0.4*</i>
	Epi	4.3 ± 0.0	9.7 ± 0.3	9.2 ± 0.4*	9.1 ± 0.9*	7.5 ± 1.0*	<i>4.4 ± 1.0</i>	<i>1.8 ± 0.7</i>	<i>0.5 ± 0.4*</i>
3	Endo	3.3 ± 0.0	9.2 ± 0.2	9.6 ± 0.3	12.0 ± 0.4	10.7 ± 0.2	<i>1.7 ± 0.0</i>	<i>2.3 ± 0.0</i>	<i>1.3 ± 0.0</i>
	Mid	3.3 ± 0.0	8.7 ± 0.2	7.9 ± 0.5*	10.2 ± 0.7*	9.7 ± 0.5	<i>1.7 ± 0.0</i>	<i>2.3 ± 0.0</i>	<i>1.3 ± 0.0</i>
	Epi	3.3 ± 0.0	8.8 ± 0.3	6.8 ± 0.4*	7.6 ± 0.7*	6.5 ± 1.0*	<i>1.5 ± 0.2</i>	<i>1.4 ± 0.4*</i>	<i>0.5 ± 0.2*</i>
4	Endo	5.0 ± 0.0	11.1 ± 0.3	11.4 ± 0.3	14.1 ± 0.2	8.2 ± 0.1	8.0 ± 0.1	<i>1.3 ± 0.0</i>	<i>0.8 ± 0.2</i>
	Mid	5.0 ± 0.0	10.7 ± 0.5	10.0 ± 0.4*	12.1 ± 0.8*	7.8 ± 0.5	7.5 ± 0.4	<i>1.2 ± 0.1</i>	<i>0.8 ± 0.2</i>
	Epi	5.0 ± 0.0	9.3 ± 0.7*	7.1 ± 0.4*	8.1 ± 0.9*	6.8 ± 0.8	5.8 ± 0.8*	<i>1.2 ± 0.2</i>	<i>0.8 ± 0.2</i>
5	Endo	5.0 ± 0.0	10.5 ± 0.2	11.1 ± 0.3	13.4 ± 0.2	14.9 ± 0.5	12.7 ± 0.6	11.0 ± 1.1	<i>0.0 ± 0.0</i>
	Mid	5.0 ± 0.0	9.8 ± 0.3*	9.6 ± 0.3*	10.0 ± 1.1*	9.5 ± 1.2*	8.0 ± 1.1*	6.0 ± 1.6*	<i>0.0 ± 0.0</i>
	Epi	5.0 ± 0.0	9.1 ± 0.3*	7.7 ± 0.4*	8.0 ± 0.7*	7.6 ± 0.8*	5.6 ± 1.0*	3.6 ± 1.1*	<i>0.0 ± 0.0</i>
6	Endo	4.7 ± 0.0	9.8 ± 0.3	10.8 ± 0.2	13.9 ± 0.0	12.5 ± 0.1	<i>1.3 ± 0.0</i>	<i>6.1 ± 0.1</i>	<i>2.3 ± 0.5</i>
	Mid	4.7 ± 0.0	9.9 ± 0.2	9.8 ± 0.2*	13.0 ± 0.5	11.4 ± 0.6	<i>1.5 ± 0.2</i>	<i>4.5 ± 0.8*</i>	<i>1.8 ± 0.4</i>
	Epi	4.7 ± 0.0	9.0 ± 0.2*	7.7 ± 0.4*	9.1 ± 1.0*	8.2 ± 0.8*	<i>1.4 ± 0.2</i>	<i>2.0 ± 0.6*</i>	<i>1.1 ± 0.4</i>
7	Endo	4.8 ± 0.0	11.8 ± 0.1	12.1 ± 0.2	15.8 ± 0.6	16.7 ± 0.6	8.3 ± 0.0	<i>7.8 ± 0.1</i>	<i>2.4 ± 0.3</i>
	Mid	4.8 ± 0.0	11.6 ± 0.1	11.2 ± 0.5	15.1 ± 0.7	16.3 ± 0.9	8.3 ± 0.4	<i>7.2 ± 0.7</i>	<i>2.1 ± 0.5</i>
	Epi	4.8 ± 0.0	11.2 ± 0.2*	9.9 ± 0.6*	12.7 ± 1.0*	11.5 ± 1.2*	6.5 ± 1.0	<i>4.4 ± 1.2*</i>	<i>1.2 ± 0.4*</i>

*P<0.05 by paired *t* test when compared with Endo average AR at same time point within same study. Data obtained after the end of the VF episode, apparent through ECG observation, are italicized.

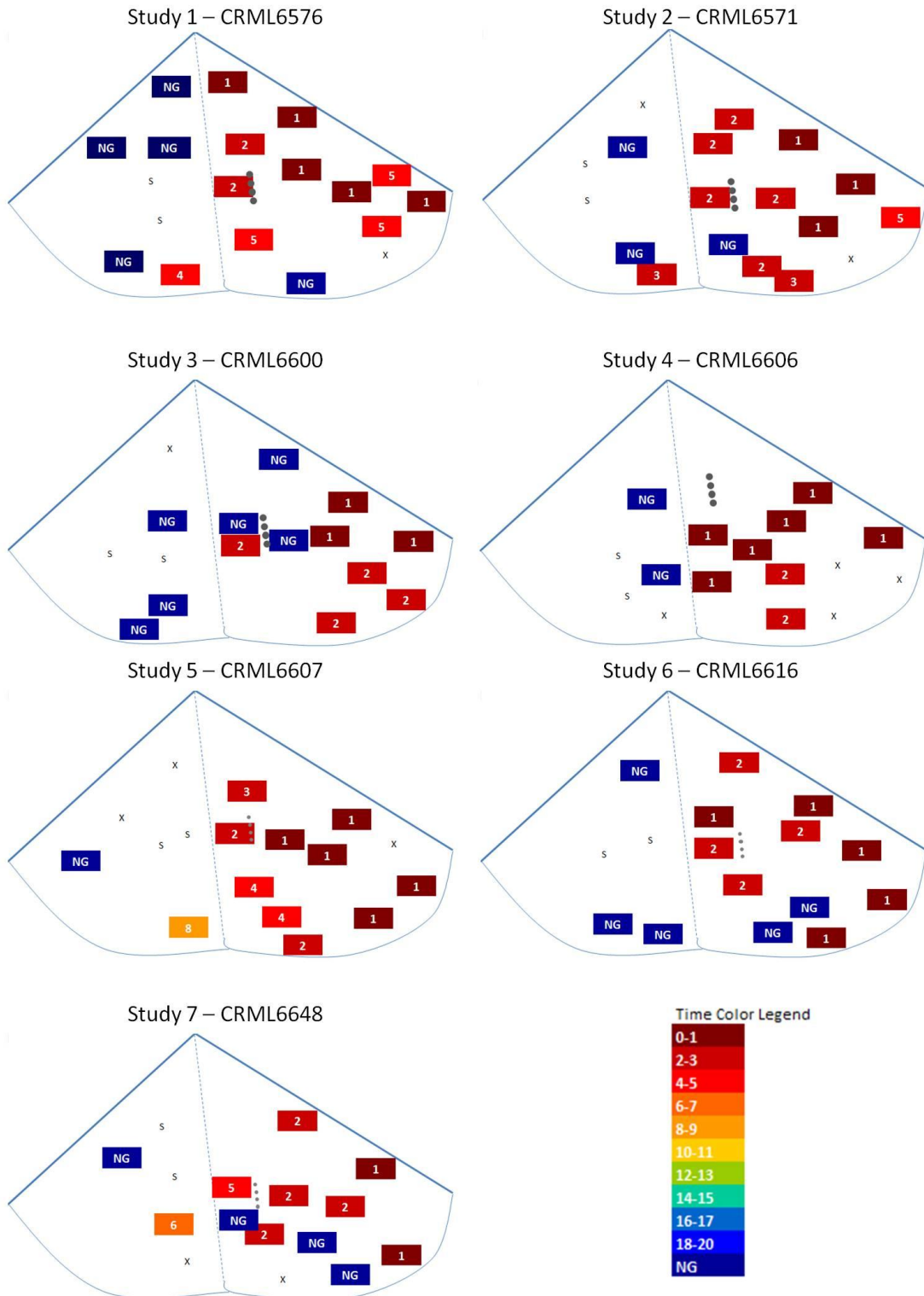


Figure 14: Ventricular heart maps showing time of gradient onset for all LDVF studies. “X” marks sites where a gradient could not be assessed due to poor signal quality. “S” marks the location of wires sutured to the RV for AC stimulation. Linear array of 4 gray circles represents the location of the resistivity needle array. The legend on the lower right lists each minute and corresponding color.

Heterogeneous Development of ARG

The development of the gradient is heterogeneous in the rabbit. In the same rabbit, sites within the LV develop an activation rate gradient at different points in time. At 3 minutes of LDVF (Figure 15), the AR of the Endo and Epi at the posterior LV site is similar (8.7Hz vs. 8.7Hz, not significant) and no gradient is present. At the lateral LV site the Epi AR is significantly longer compared to the Endo (8.7Hz vs 6.7Hz respectively, $p < 0.05$). Table 3 summarizes the heterogeneity of gradient development within each study. While each heart had at least one LV site to present a gradient at the time of the first activation rate measurement (obtained immediately after the end of AC stimulus), 3 of 7 hearts had a range of gradient onset times equal to 4 minutes. Five of 7 hearts had at least one site in which no sustained AR gradient was present. Gradient onset maps for each study show time of gradient onset for all sites during LDVF (Fig 14).

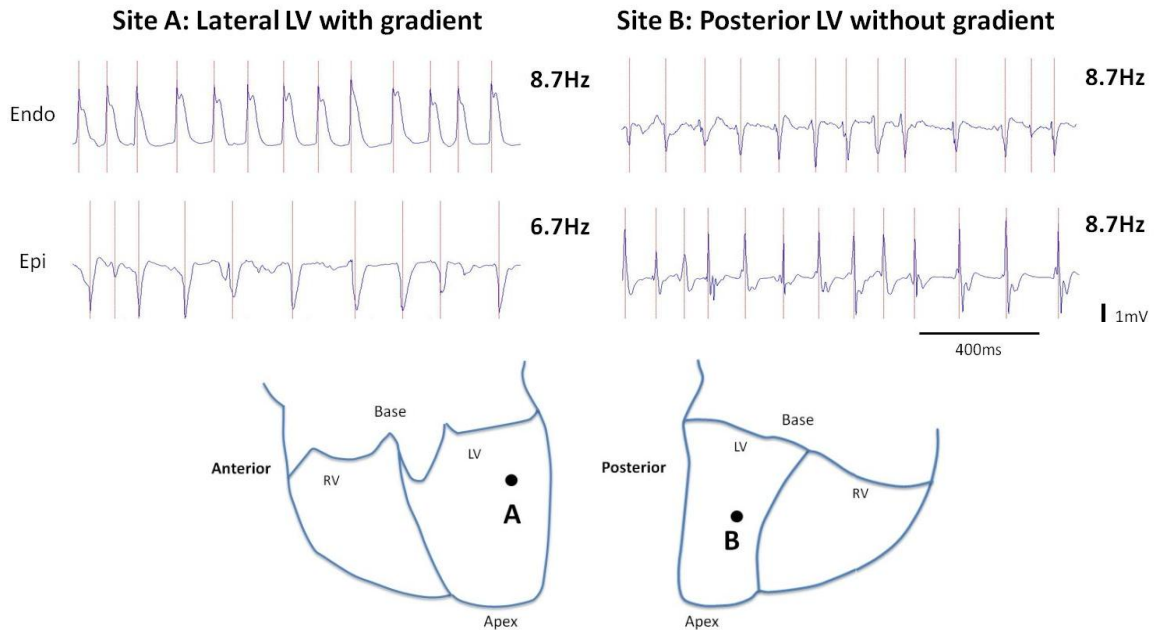


Figure15: Endo and Epi electrograms from two plunge needles in the same heart at 3min after VF onset. A schematic of the ventricles is included below the electrograms to illustrate the location of each plunge needle. At the lateral LV site the Epi AR is significantly longer compared to the Endo. The AR of the Endo and Epi at the posterior LV site is similar and no gradient is present.

Table 3
Activation Rate Gradients Observed in LV Sites During LDVF

Study	Average Gradient Onset (min)	First Gradient Onset (min)	Range of Gradient Onset (min)	Sites with no sustained gradient	Total LV Sites
1	1	1	4	1	11
2	2	1	4	1	11
3	2	1	1	3	10
4	1	1	1	0	8
5	1	1	3	0	10
6	1	1	1	2	11
7	1	1	4	3	11

Observation of the development of the ARG with respect to ventricular region revealed differences between the apical area and more basal areas for the LV. The mean time to gradient onset was significantly later in the LV apex (2.8 ± 0.4 min) compared to the LV base and mid (1.6 ± 0.2 and 1.9 ± 0.2 min, respectively) as shown in Figure 16A. All LV sites which would develop an ARG had developed the gradient within 5 minutes of LDVF. Figure 16B shows that the basal LV had the most sites to develop a gradient (96%, n=26 sites), followed by the Mid LV (84%, n=32 sites). The apical LV had 69% of sites (n=13) with an ARG and was the LV area most prone to have sites that did not develop a gradient. There were no sites in the RV base (n=6) or mid (n=3) to develop an ARG. In the RV apex, 36% (n=11) of sites developed the gradient by 10min of LDVF with the average time to gradient onset being 5.3 ± 1.1 min.

Activation not only revealed spatiotemporal heterogeneous gradient development, sites of inactivity appeared during times when the surrounding area retained activity. Figure 17 displays electrograms from 3 neighboring Epi sites at 11 minutes of VF from a representative rabbit. Site B has no deflections with magnitude greater than 0.25mV and is found to be inactive while nearby sites A and C remain active.

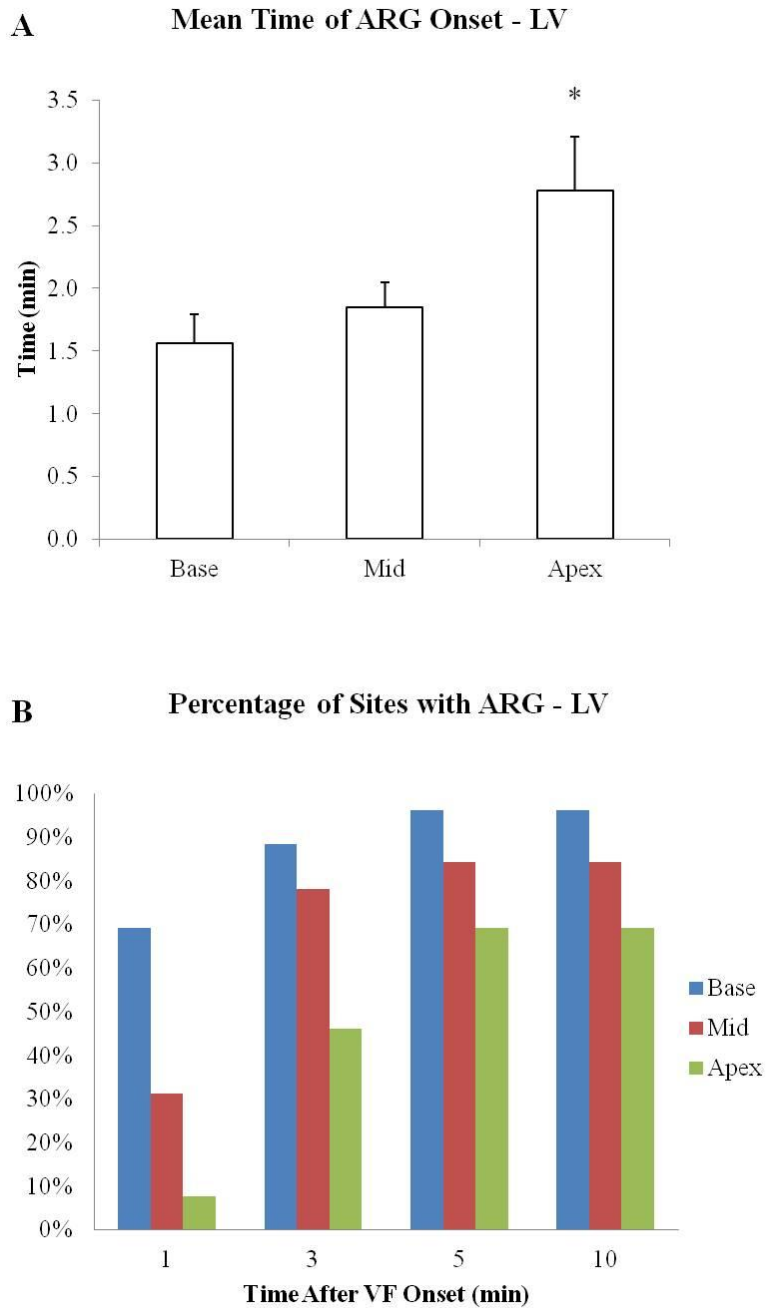


Figure 16: Mean time of ARG onset is shown for the basal (Base), middle (Mid), and apical (Apex) regions of the LV (A). Data values are means \pm standard error of the mean obtained from 7 LDVF *in vivo* rabbit studies. Percentage of sites having the ARG at certain time points of LDVF is shown for the Basal, Middle, and Apical regions of the LV (B) from the same LDVF studies.

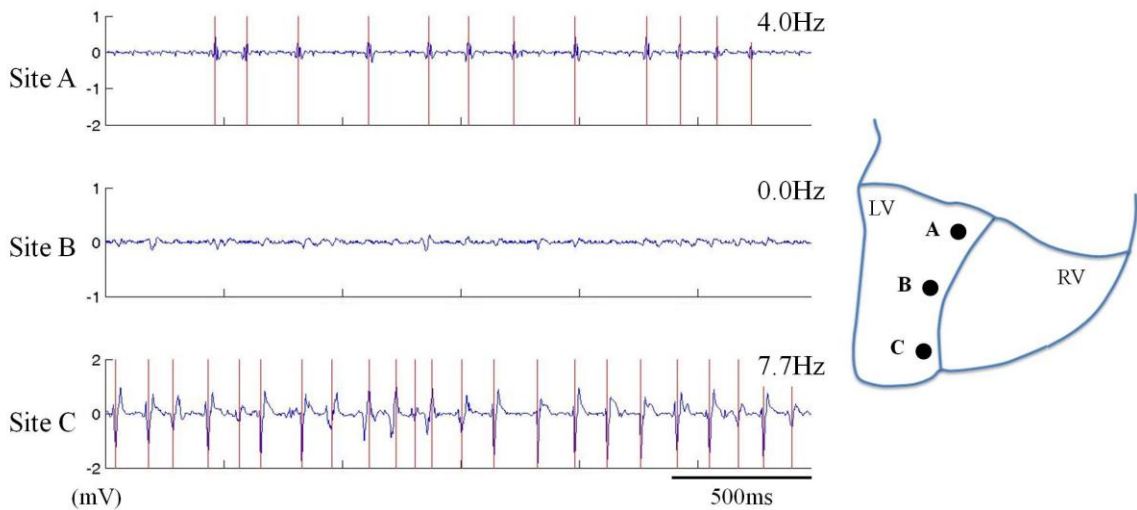


Figure 17: Epicardial electrograms from 3 sites at the posterior LV of a representative rabbit study are shown during 11min of VF. Activation rate is displayed at the top right of each electrogram. A diagram indicating the location of each site is shown to the right of the electrograms. Site B becomes inactive at 11min of VF while neighboring sites A and C retain excitability.

Analysis was performed to determine whether the activation rate gradient was a result of Epi inability to attain rapid activation rates below a certain threshold rate. There was only 1 Epi site at one point in time for 2 VF studies in which an Epi site reached a maximal AR equivalent to the maximal Endo AR. In the other 5 studies, the difference between the maximum AR achieved by any Epi site compared to Endo sites ranged 2.3-5.6Hz. Despite the fact that Epi rarely achieved maximal Endo rates, there was no threshold Endo activation rate to result in the Endo-Epi gradient. Endo AR are shown from 3 sites in 2 VF studies in Figure 18. In Figure 18A, AR is similar and no gradient has developed at SR or 1 minute VF for all 3 sites. At 2 minutes VF, sites 1 and 2 have developed a gradient when Endo AR reaches 12.3Hz and 11Hz, respectively. However, site 3 has not developed a gradient even though Endo AR has reached 11.7Hz. The ARG persists in sites 1 and 2 for the duration of LDVF. Although Endo AR progresses to a rate of 13.3Hz, rates for which an ARG occurs in sites 1 and 2, an ARG does not develop in

site 3. Figure 18B displays AR for site 1 which develops an ARG at 1 minute of VF and sites 2 and 3 which develops an ARG at 5 minutes of VF. At 1 minute VF, AR at site 1 (13Hz) is greater than AR at sites 2 and 3 (10.3Hz and 11.7Hz, respectively) and a gradient has developed and persists for the remainder of VF. Although Endo AR in site 3 surpasses that in site 1, an ARG does not develop until 5 minutes of VF when Endo AR reaches 20.3Hz. These representative sites demonstrate that the gradient does not develop due to Endo AR exceeding some specific rate of activation. There are rapid Endo rates for which no gradient develops, and there are slower Endo rates for which a gradient does occur. Therefore, the Endo-Epi gradient is not a rate threshold effect.

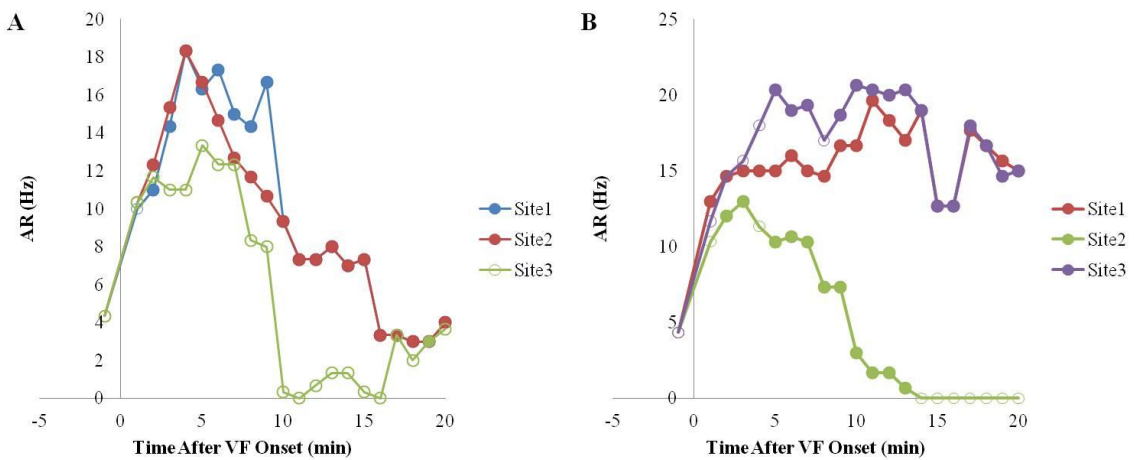


Figure 18: Activation rates are shown for each minute of VF from 2 rabbit LDVF studies (A and B) at 3 Endo sites each. Open circles indicate no Endo-Epi AR gradient, closed circles indicate the presence of an Endo-Epi AR gradient. In (A), a sustained AR gradient develops in sites 1 and 2 by 2min of VF. Site 3 does not develop a gradient. In (B), site 1 develops a sustained AR gradient by 1min while sites 2 and 3 do not sustain a gradient until 5min of VF.

To assess whether the ARG was a result of activations which did not conduct from Endo to Epi due to shorter cycle lengths, the Endo cycle lengths for activations which conducted from Endo to Epi were compared to Endo cycle lengths for activations which did not conduct to the Epi from selected sites of each study. There was no significant difference between the average of cycle lengths for activations which

conducted compared to those which did not. There was also no minimum Endo cycle length for which the Epi would not activate. Average Endo cycle length for activations which conducted from Endo to Epi compared to activations which did not conduct to Epi are shown for the first 5 minutes of VF from a site in a representative rabbit LDVF study in Figure 19. In this study and at this site, an ARG developed by 1 minute of VF. There was no significant difference between cycle length for any time point. By 4 minutes of VF, average cycle length for non-conducted activations were very short, but cycle length of conducted activations were similarly short (40.2 ± 1.0 vs. 45.4 ± 2.0 , $p=NS$). These results indicate that the gradient is not simply a consequence of Epi inability to activate in response to Endo activations with short cycle lengths, further indicating no threshold effects.

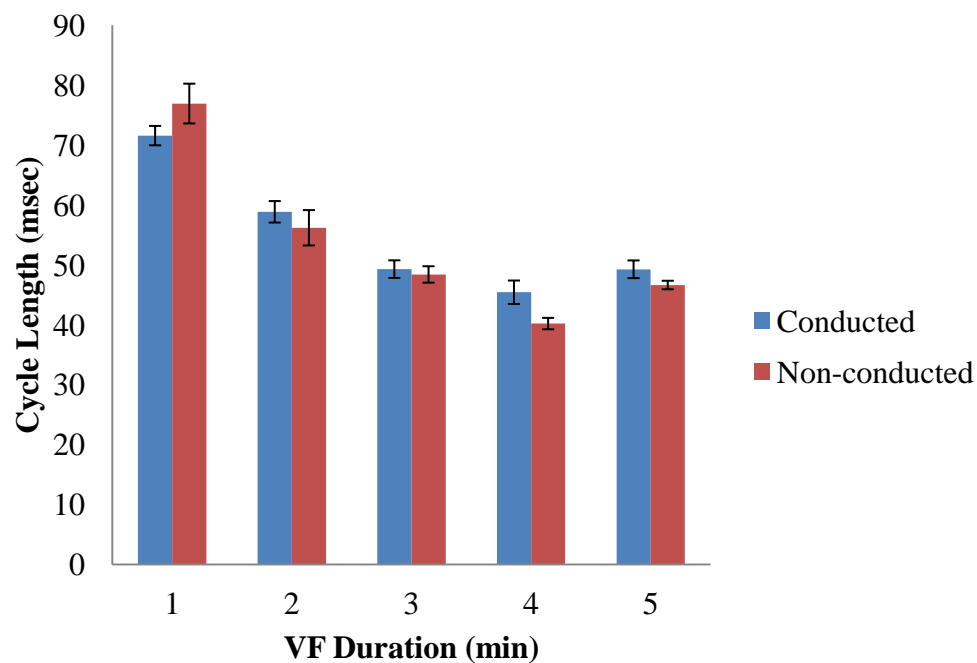


Figure 19: Average Endo cycle length for activations which conducted from Endo to Epi compared to activations which did not conduct to Epi for the first 5 minutes of VF from a site in a representative rabbit LDVF study. Standard error bars are included. There was no significant difference between average cycle lengths at any time point.

Resistivity

Voltage Response Assessment for Resistivity Measurement

Myocardial resistivity was measured using a four electrode resistivity technique to deliver a subthreshold direct current consisting of rectangular pulses of alternating polarity ($\pm 10\mu\text{A}$, 10ms pulse width, 200ms delay) across the outer electrodes of each array and concurrently recording potential difference between the inner electrodes of each array. The voltage response of the myocardial layer from each current pulse was contained in voltage recordings. I designed an algorithm in MATLAB to take a user input of the time location of the first positive voltage response, create a measurement window based on the pulse width, measure the magnitude of the rise and fall of the pulse, and then progress forward in time equal to the pulse delay after each measured pulse. Pulse onset time is the point before the onset of rapid rise of the voltage response. Voltage response magnitude is measured as the voltage after a rise time of 1.5ms minus voltage at pulse onset. Since pulse onset time is entered for the first positive pulse, the algorithm separates every other pulse into a matrix of positive voltage response values and negative voltage response values. Average voltage response is determined by the average of voltage response magnitudes from all positive pulses.^{33,37}

Voltage Response Selection Criteria

Measurement of resistivity using DC current with the four electrode resistivity technique during VF presented the challenge of resolving voltage responses that overlapped with rapid cardiac activations. This problem resulted in initial difficulty in accurately selecting pulse onset time and distortion of the measured pulse magnitude. As

a solution, a set of algorithms were developed which use a combination of evaluation of voltage response characteristics and high pass filtering in order to only include square pulses that are largely unaffected by local activations. All data is subjected to an online high pass filter of 0.5Hz during data acquisition and recording. The application of a high pass filter (HPF) mentioned through out the rest of this document refers to an offline filter applied to the data during data analysis. High pass filtering with a cutoff frequency of 40Hz was incorporated to remove low frequency components within the electrogram, especially that of the activations, thereby reducing activation width and increasing the quiescent time between activations for square voltage responses to occur. Through the use of this filter, identification of the pulse onset time is made more clear resulting in accurate selection of pulse onset time and proper alignment of the analysis window with the pulse location. Data from a representative rabbit analyzed using HPFs with cutoff frequencies of 10Hz, 20Hz, 30Hz, and 40Hz is shown in Figure 20B. While the HPF attenuated the magnitude of the voltage response as well as the activations, the decrease in voltage response magnitude was less than 10% even at an HPF with 40Hz cutoff frequency (Figure 21) and the measured relative change in resistivity was largely unchanged (Figure 20B). Response characteristics exclusions were developed through evaluation of the effects activation overlap has on voltage response characteristics and were applied to each pulse analyzed. Exclusions include:

$$BmA < 0 \text{ OR } CmD < 0$$

$$amA < 0 \text{ OR } amA < 0.1 * BmA$$

$$BmA > \overline{BmA} + 2\sigma \text{ OR } BmA < \overline{BmA} - 2\sigma$$

$$DmA > \overline{DmA} + 2\sigma \text{ AND } (BmA > \overline{BmA} + \sigma \text{ OR } BmA < \overline{BmA} - \sigma)$$

$$|DmA| > 0.5mV$$

Refer to Figure 22 for a further description of variables. The use of these exclusions removes a majority of outlier pulses from all data analyzed in a consistent fashion and without user bias. Figure 20 shows results of data analysis with (Figure 20C, 20D) and without exclusions (Figure 20A).

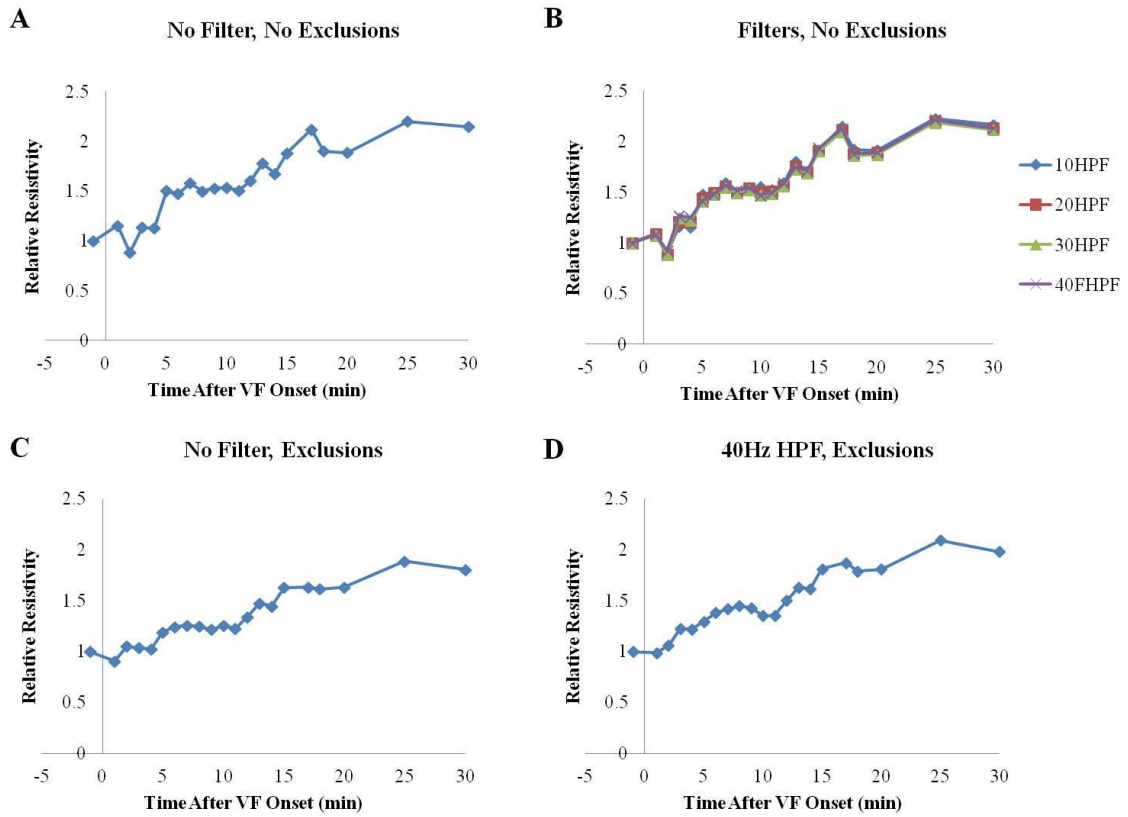


Figure 20: Data analysis of resistivity from the Endo level (L3) of a representative rabbit using high pass filtering and points of exclusion. Relative resistivity values from analysis (A) with no high pass filter or exclusions applied, (B) when high pass filters with cutoff frequency ranging from 10-40Hz are applied, (C) when all points of exclusion are applied, and (D) when all points of exclusion and a high pass filter with cutoff frequency of 40Hz are applied. In plot B, each color line represent a different high pass filter applied.

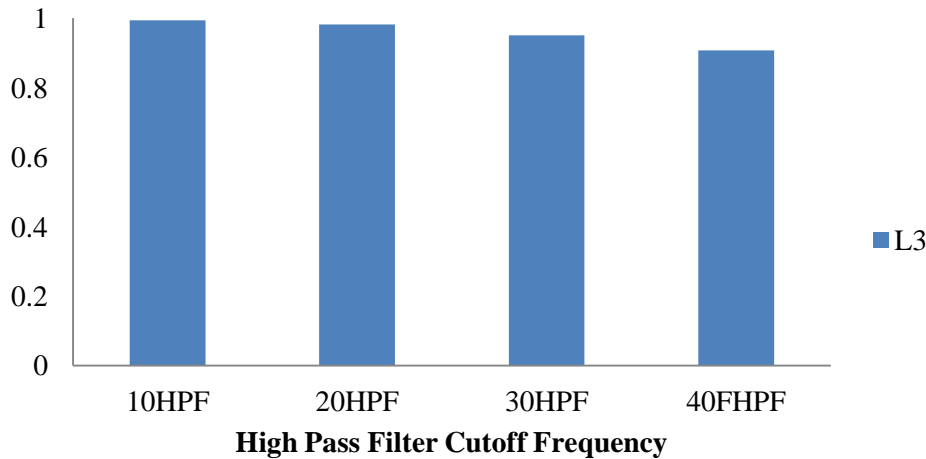


Figure 21: Bar graph of the attenuation of the original unfiltered data by the application of high pass filtering with cutoff frequency ranging from 10-40Hz in the Endo level (L3) of myocardium from a representative rabbit.

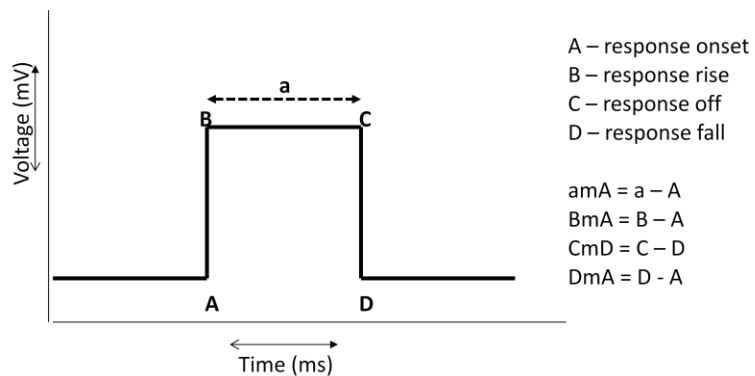


Figure 22: Schematic of a voltage response to a square current pulse. Points of the voltage response are labeled for reference in response characteristic calculations. The value “a” is the average of voltage response values between the response rise and response off time.

Stability of Electrode Array

The stability of the electrode array is shown in data measured during 60 minutes of SR preceding VF onset. Relative resistivity values (n=3), shown in Figure 23, remain stable over the 60 minute time period with less than 9% change in any array level. These results indicate that the electrodes remain stable over the course of the experiment and have little to no impact on the resulting resistivity values observed in the myocardium.

Average baseline resistivity during SR is plotted in Figure 24. The average values seen in the Endo, Mid, and Epi levels (287 Ωcm , 468 Ωcm , and 461 Ωcm respectively) are within the range of values other groups have measured.^{33,37,38} The average value observed in the cavity level array during SR (81 Ωcm) is well below our observed values in tissue and also below that observed by other groups. The difference in resistivity allows for distinction between the tissue and the ventricular cavity and confirmation that our tissue level arrays, especially the endocardial array, is truly in tissue.

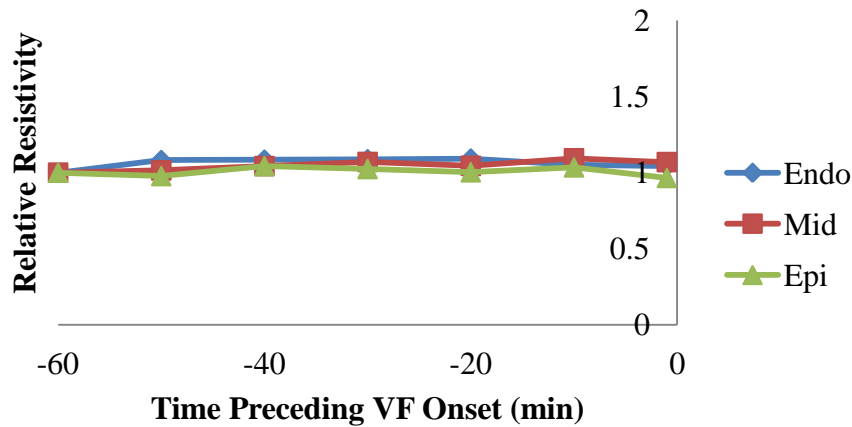


Figure 23: Average relative resistivity of rabbit LV (n=3) during 60 minutes of SR in three resistivity array levels: Endo (L3), Mid (L4), and Epi (L5). Time 0min represents the time when VF begins. Time -60min represents SR, 60min prior to VF. Recordings were made every 10min and also 1min before VF onset.

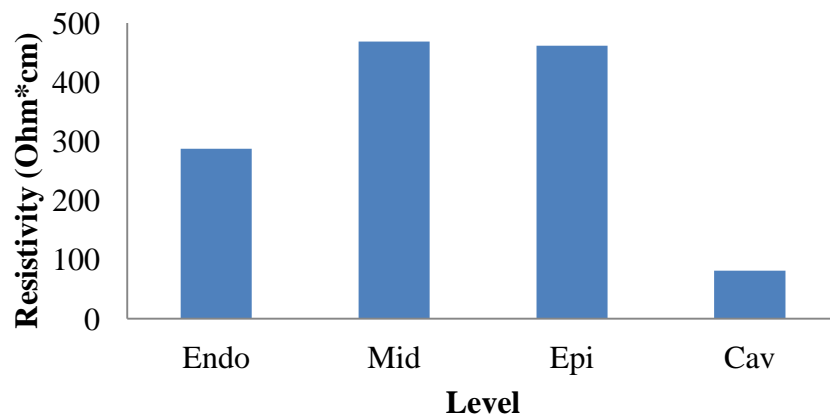


Figure 24: Average resistivity of rabbit LV (n=3) in four resistivity array levels at baseline (SR). The four arrays are identified in the chart legend as Endo (L3), Mid (L4), Epi (L5), and Cav (L1). Resistivity in the cavity level array was, as expected, much lower than that of the tissue level (Endo, Mid, Epi) level arrays.

Resistivity Measurement Does Not Alter VF Activation Rate

Measuring resistivity using the four-electrode resistivity technique requires that current be injected into the myocardium frequently in order to observe minute by minute changes that occur during LDVF. To determine whether the selected current magnitude imposed any changes in the rate or progression of VF, a comparison of activation rate was performed between studies with the resistivity array (n=3) and without the resistivity array (n=3) for the Endo and Epi levels (Figure 25). There was no significant difference found in activation rate for either level at any time point examined. Therefore, the insertion and use of the resistivity array does not change the course of VF.

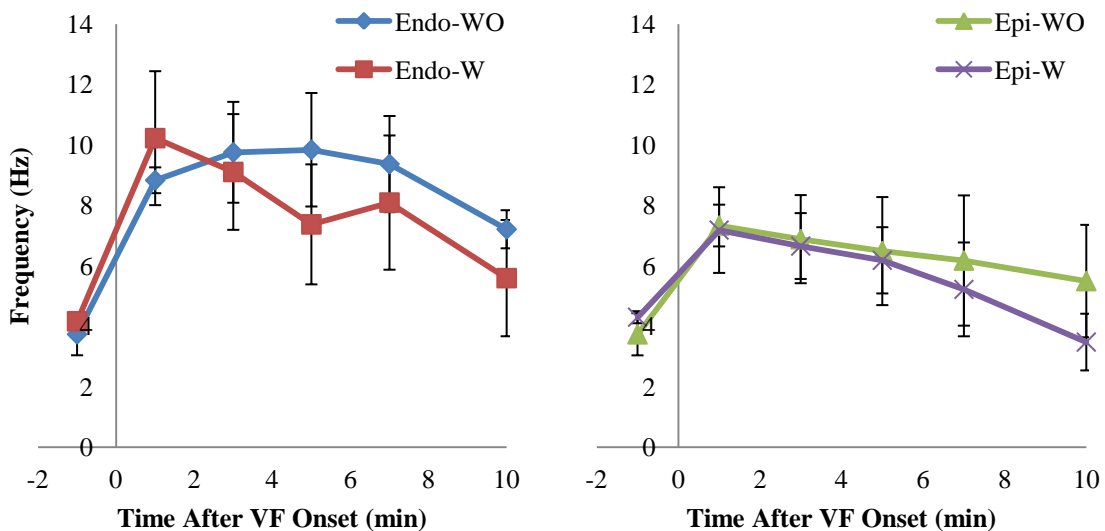


Figure 25: Frequency of activation during LDVF with and without insertion of a resistivity array in the (left) Endo and (right) Epi. Standard error bars are included for each point in time. There was no significant difference in activation rate between hearts with (W) and without (WO) the resistivity array for the Endo or the Epi levels.

Characteristics of Transmural Changes in Intramural Resistivity

All resistivity values were normalized (referred to as relative resistivity) in order to permit data comparisons between myocardial layers of each heart as well as

comparisons between all hearts. Relative resistivity for each myocardial layer in each study was calculated as the ratio of each resistivity value to the value of resistivity obtained during SR just prior to VF or ischemia induction. From this point on, any mention of resistivity refers to relative resistivity.

Resistivity data from a representative rabbit study is shown in Figure 26. Resistivity increased rapidly immediately after the onset of VF in the Epi level compared to the Endo and Mid levels. In the Mid level, resistivity exhibits a more gradually rate of increase after VF onset. Very little change in resistivity was seen in the Endo level from baseline to 11 minutes of VF. After that time point, a steep increase in resistivity occurred. By 10 minutes, relative resistivity increased 1.36 fold in the Epi, 1.17 fold in the Mid, and there was only minimal change from baseline in the Endo. By 20 minutes of VF, both the Epi and Mid have peaked at 1.6, however, the Endo never reaches this magnitude of relative change and peaks at only 1.37. The differential resistivity changes observed qualitatively across the Endo, Mid, and Epi in this study supports the idea of altered coupling as a basis for development of transmural gradient.

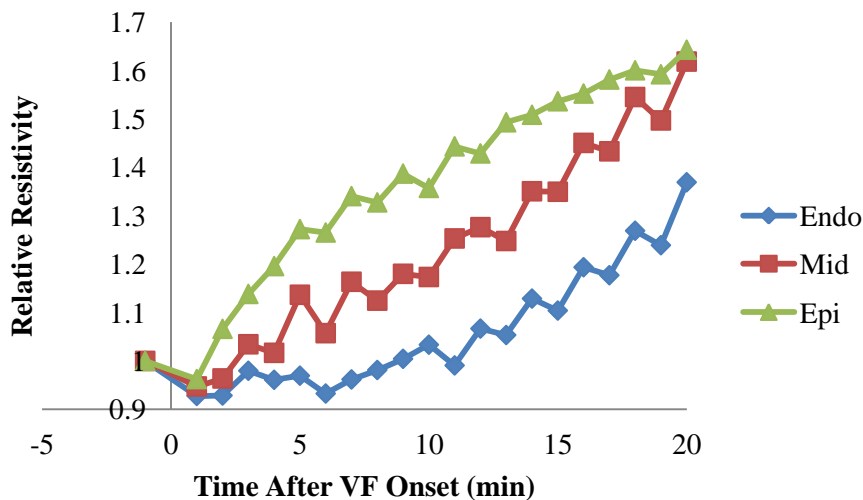


Figure 26: Relative resistivity for the Endo, Mid, and Epi layers shown for 1-20min after induction of long-duration VF in a representative rabbit study.

Changes Observed in Relative Resistivity

Qualitatively, resistivity profiles in the Endo, Mid, and Epi consisted of only a single prominent rise in most cases of LDVF, whereas resistivity profiles during ischemia consisted of an immediate rise followed by a significant, steep secondary rise. Analysis of the relationship between resistivity and activation rate obtained during LDVF revealed that a steep increase in resistivity often occurred during the time of marked changes or events in activation rate. Subsequently, the definition of uncoupling used by Jain et al. was modified and stated for this study as follows: The onset of the steep rise in resistivity occurs when a 5% increase in relative resistivity from the previous resistivity measurement is observed, the average of the subsequent 3 values demonstrates a 3% increase, and resistivity sustains a relative value of 1.0 or greater. This definition was designed as more stringent criteria to avoid premature labeling of the steep resistivity rise onset due to transient fluctuations in resistivity measurements that transpire during VF measurement. The time of steep resistivity increase for the Endo, Mid, and Epi layers in each study are listed in Table 4. In all but one *in vivo* LDVF study, steep rise onset times occurred progressively with Epi onset before or concurrently with Mid, and Mid before Endo. In Study 3, VF duration was 6 minutes which would make the Mid and Endo onset times (14min and 17min, respectively) invalid. In study 7, resistivity analysis determined Epi onset time to be simultaneous with Endo onset time. It is possible that signal noise or overlap with activations caused disruption of the resistivity profile resulting in a less precise calculation of steep resistivity rise onset time. In Study 6, the LV wall was too thin (approximately 3.2-3.8mm) to obtain Endo resistivity measurement. During the course of LDVF, the average time of Epi steep resistivity rise onset (4.4 ± 1.5 min) was

earlier than Mid onset (7.3 ± 1.5 min, p value not significant) and significantly earlier than Endo onset (12.7 ± 1.2 min, $p < 0.01$). Also, Mid onset occurred significantly earlier compared with Endo onset time ($p < 0.05$). Mean values at the time of steep resistivity rise onset in the Endo, Mid, and Epi were 1.12 ± 0.03 , 1.11 ± 0.04 , and 1.16 ± 0.03 respectively.

Table 4			
Time of Intramural Steep Resistivity Rise Onset			
Study	Endo	Mid	Epi
<i>Ventricular Fibrillation</i>			
1	11	7	1
2	12	3	2
3	17	14	3
4	12	11	11
5	15	4	1
6		5	4
7	9	7	9
<i>In vitro Global Ischemia</i>			
1	36	22	
2	48	28	

The differential rate of change in resistivity during LDVF is presented in Figure 27 which shows the mean relative resistivity at each time point for the Endo, Mid, and Epi layers. Epi rapidly increases immediately after VF onset and has a significantly greater rate of increase compared to the Endo ($p < 0.05$). The rate of increase reaches or exceeds 5% per minute at 1, 7, and 12 minutes for the Epi, Mid, and Endo respectively. The steep rate of resistivity increase exhibited by the mean data is very similar to the mean onset times for the steep rise in resistivity observed across studies individually.

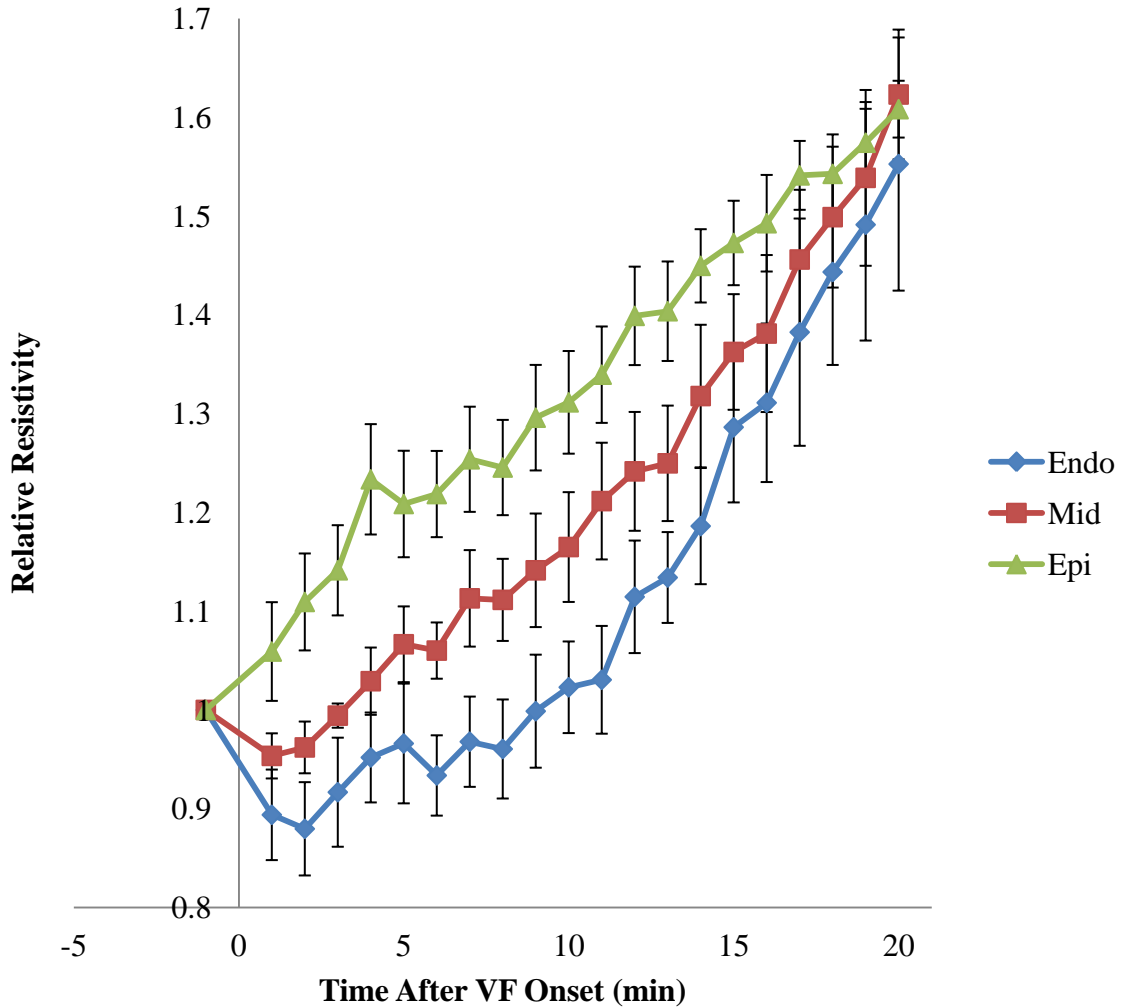


Figure 27: Relative resistivity for the Endo, Mid, and Epi myocardial layers is shown during the course of LDVF. Data values are means \pm standard error of the mean obtained from 7 LDVF *in vivo* rabbit studies (n=6 for Endo, n=7 for Mid and Epi).

Resistivity measurements during global ischemia in the *in vitro* preparation revealed that Mid steep resistivity rise onset occurred prior to Endo onset (25 ± 3 min vs. 42 ± 6 min, respectively). Average relative resistivity values at the time of onset were 1.57 ± 0.1 in the Mid and 1.61 ± 0.21 in the Endo. Resistivity for the Epi could not be assessed due to exposure of the Epi level resistivity array to the surrounding Tyrode's solution. Steep resistivity rise onset in all layers occurred much sooner during VF than rise onset for the Endo or Mid during global ischemia. Resistivity data from a

representative LDVF study and a representative global ischemia study is shown in Figure 28. Resistivity increases proceed much more quickly during LDVF compared with global ischemia. Very minimal change develops during global ischemia even by 20 minutes (see inset of Figure 28B) whereas steep rise onset during LDVF occurs by 2, 3, and 12 minutes in the Epi, Mid, and Endo respectively. Steep rises do not occur in global ischemia until 22 minutes in the Mid and 36 minutes in the Endo. This quantitative assessment of myocardial resistivity demonstrates the occurrence of differential transmural increases in resistivity in both LDVF and global ischemia.

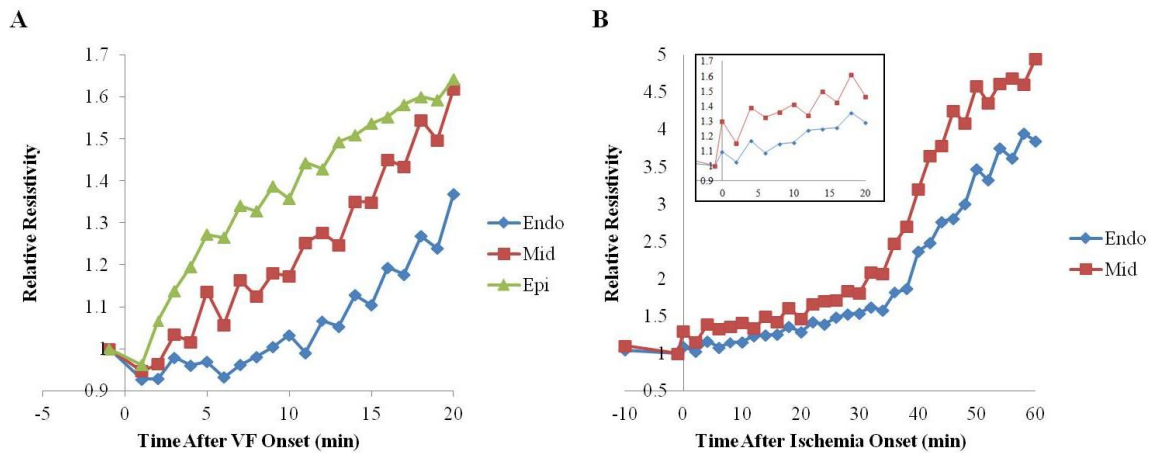


Figure 28: Relative resistivity is shown from (A) a representative *in vivo* rabbit study for 20min following induction of VF in the Endo, Mid, and Epi layers and (B) a representative *in vitro* rabbit heart study for 60min following global ischemia induced by cessation of perfusion in the Endo and Mid layers. An inset shows the same resistivity data for global ischemia plotted only from 0-20min with a similar relative resistivity scale as plot A.

Relationship Between ARG and Resistivity in LDVF

Average intramural activation rate and intramural relative resistivity for the Endo, Mid, and Epi layers are plotted side by side for 3 studies of LDVF performed (Fig 29). Onset of the steep rise in resistivity is indicated as a large black data point for each intramural layer in each relative resistivity plot. Changes in intramural relative resistivity

closely related to changes in activation rate in most instances. In Figure 29A, onset of Epi steep resistivity rise (determined as a 5% increase in resistivity with subsequent 3% increase) occurred at 2 minutes of VF. This same point in time is when the ARG developed between the Endo and Epi. Onset of steep rise in the Mid occurred by 3 minutes of VF and at the same time point an ARG developed between the Endo and Mid. At 12 minutes of VF, the Endo layer experienced onset of the steep resistivity rise. This closely followed the time when a substantial slowing in AR occurred in the Endo. A separation in the profiles of relative resistivity presented with rapid Epi rise, moderate mid rise and slower time to Endo rise. In Figure 29B, onset of Epi steep resistivity rise and the Endo-Epi ARG develop at 1 minute of VF. An ARG develops between the Mid and Endo by 3 minutes of VF. After 5 minutes Mid AR begins to decline. Shortly thereafter, Mid steep rise onset occurs at 7 minutes of VF. Endo steep rise onset occurs by 11 minutes preceding a substantial slowing in Endo AR at 15 minutes of VF. Qualitatively, Epi resistivity has a rapid rise while Mid and Endo progress closely together with a moderate time to rise. Figure 29C displays AR and resistivity for a study in which VF only sustained for 6 minutes. Epi steep resistivity rise onset at 3 minutes shortly follows the development of the Endo-Epi ARG at 2 minutes. Epi resistivity rises more quickly compared to Mid and Endo resistivity which progress with similar relative increase. Mid and Endo steep rise onset did not occur until after VF converted to pulseless electrical activity. The steep rise in resistivity in these layers were attributed to ischemia following the 6 minute VF episode. The 3 studies outlined in Figure 29 are representative of the relationships between intramural ARG and resistivity which occurred in all LDVF studies performed. Table 5 shows the time of Epi steep resistivity

rise onset and time of ARG development. There was a significant difference in average Epi steep rise onset time compared to average ARG time of development ($4.4 \pm 1.5 \text{min}$ vs. $1.29 \pm 0.18 \text{min}$), however, these times only differed by 3.1min. Therefore, the time when the steep rise in Epi resistivity occurs closely follows the time when a significant difference in activation rate develops between the Endo and Epi.

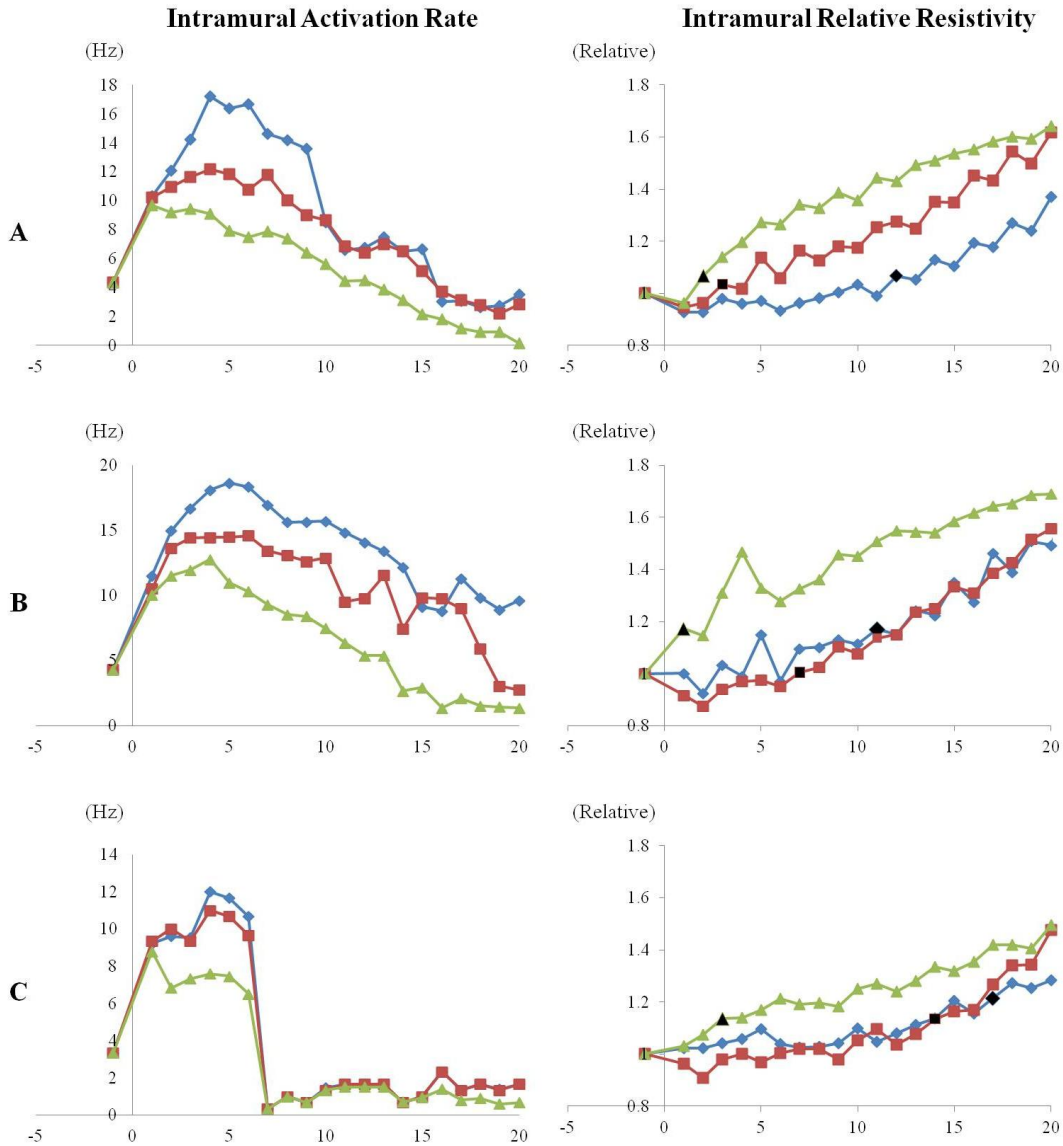


Figure 29: Average intramural activation rate (on left) and intramural relative resistivity (on right) are shown for the Endo, Mid, and Epi layers in 3 studies of LDVF in rabbit. In each relative resistivity plot, black data points indicate the onset time of steep resistivity rise for each intramural layer.

Table 5		
Epicardial Steep Resistivity Rise Onset vs. Activation Rate Gradient Onset		
Time After VF Onset (min)		
Study	Epi Uncoupling	ARG
1	1	1
2	2	2
3	3	2
4	11	1
5	1	1
6	4	1
7	9	1
Average	4.43	1.29
Standard Error	1.51	0.18

DISCUSSION

Discussion of Results

This project has investigated the mechanisms of the activation rate gradient which develops during LDVF. In summary, we developed a novel preparation of LDVF in the *in vivo* rabbit heart, demonstrated that an activation gradient develops with similar time course as in dog, developed and validated a method using a plunge needle resistivity array to assess transmural changes in resistivity, delineated the time course of the activation rate gradient with steep resistivity increases during LDVF, and utilized *in vitro* control studies to demonstrate our transmural resistivity results to be comparable with previously documented ischemia results and reveal a dissimilarity of resistivity steep rise time course in VF compared with myocardial ischemia. The major finding of this project is the development of differential transmural increases in resistivity in the left ventricular myocardium with steep rise onset progressing from Epi to Endo. Particularly, the steep rise in epicardial resistivity developed earliest and was closely associated with the development of the Endo-Epi activation rate gradient. Steep rises in resistivity developed much more quickly during LDVF than during myocardial ischemia.

VF Induction

Long-duration VF was most successfully obtained in rabbits weighing 3.3kg or greater using an AC stimulus of 60s duration. Due to the fact that a critical size of myocardium of at least 100-400mm² is necessary to sustain fibrillation,^{39,40} and that the rabbit heart is at the crux of this critical size, investigation in rabbit presented a challenge

to consistently obtain sustained VF. Larger rabbits with larger hearts yielded a higher likelihood to develop sustained VF. Despite improved probability, it was still necessary to use the prolonged current to sustain VF even in the larger hearts as demonstrated in Figure 5. Our review of the literature did not find a study citing VF induction methods in the *in vivo* rabbit heart; the majority of VF studies have been performed in *in vitro* preparations. This stimulation protocol is substantially longer what others have used in those *in vitro* rabbit heart preparations;^{15,16,41,42} however, electrophysiological properties differing between the *in vivo* and isolated preparations likely demand a more rigorous protocol to obtain sustained fibrillation in the *in vivo* rabbit heart. Adult rabbit hearts (of rabbits greater than 3.3kg) consistently developed LDVF with 60s stimulation creating an intriguing model with which to assess VF.

Activation Rate Gradient

A minimum cycle length criterion of 35ms was used for activation rate calculation. A 50ms criterion is widely used with activation rate assessment in dogs^{11,34} and pigs.⁴³ However, the justification for the 50ms minimum rate criterion comes from studies on canine cardiac refractoriness. Due to the fact that rabbits have an intrinsic activation rate much faster than dogs or pigs, this minimum cycle length was reconsidered. Many studies that investigate AR in rabbit estimate the activation rate using a dominant frequency method^{15,16,17,18} which does not depend on each individual cycle length but the overall rate over time. Calculation of activation rate using an activation selection minimum cycle length criterion is highly dependant on the minimum allowable time span between activations. The decision to use a minimum cycle length of 35ms was

supported by reports of VF dominant frequency in rabbit exceeding 20Hz to values ranging 21-26Hz.^{15,16}

After selection of the lower minimum cycle length (35ms), it was necessary to implement further analysis criteria to prevent the selection of electrotonic deflections or double potentials as activations. Double potentials are two closely spaced deflections in which one or both are electrotonic activity propagating from nearby activations.⁴⁴ Double potentials are defined in canine ventricular muscle as deflections occurring less than 50ms from one another.¹¹ To prevent selection of double potentials, activations must have an isoelectric interval occurring between them. We defined an isoelectric interval as a 3ms period of 0 slope. If a double potential occurred, only the potential with the greatest absolute magnitude was selected as the activation.⁵ Activation times were assigned to the peak of activations with magnitude greater than an absolute value of 0.25mV.⁷ The use of different criteria to evaluate electrograms may lead to different rate values; however, the definitions outlined here were determined as the best fit for the data we obtained based on literature review and data analysis.

Studies on the organization of LDVF have shown the development of activation rate gradients between the LV Endo and LV Epi in the dog and rabbit.^{11,12,13,18} Gradients also develop between the RV Endo and RV Epi in the dog,¹² but not the rabbit.¹⁸ The activation rate gradient develops within 1-3 minutes of LDVF in the dog LV.^{11,12,13} In the isolated rabbit heart preparation, an Endo-Epi disparity of AR develops within 3 minutes of VF in the LV;¹⁸ however, this study only investigated rates on the Endo and Epi surface and used separate measurement techniques. Results from our investigation of *in vivo* rabbit LDVF are consistent with previously mentioned studies showing early

development of the Endo-Epi LV gradient and provide transmural data on the development of the gradient in rabbit. An Endo-Epi gradient developed in every VF study. Similar to Venable et al., we found a significant difference in rate to develop between Endo and Mid and between Mid and Epi, but in 57% of studies. There was one instance of Endo-Mid similarity and one instance of Mid-Epi similarity. There was also an instance in which there was no significant difference between adjacent layers, only an Endo-Epi difference. Based on our analysis of resistivity, the transmural heterogeneity of excitability is due to cellular electrical uncoupling. This uncoupling is likely due to heterogeneous expression and dephosphorylation of Cx43, the principle protein of gap junctions. Canine Epi has a lower expression of Cx43 compared with more endocardial layers in the ventricle⁴⁵ and this may also hold true for the rabbit ventricular myocardium. Lower expression of Epi Cx43 would lead to a faster rate of Epi electrical uncoupling should dephosphorylation (induced by concurrent fibrillation and ischemia) occur with similar extent across the myocardium. Otherwise, heterogeneous dephosphorylation of Cx43 during fibrillation may be the biochemical mechanism for the differential transmural steep increases in resistivity during LDVF in the rabbit myocardium.

Venable et al. also documented the occurrence of inexcitable areas during later periods of LDVF.¹² This study described areas of inexcitability adjacent to regions which were still active. We found that at individual sites within the LV, the gradient of activation rate developed at different points in time during LDVF. Furthermore, areas of inexcitability occurred during times when adjacent sites were still active. This pattern of gradient development further implicates heterogeneous Cx43 expression as a mechanism for altered excitability and electrical coupling.

Resistivity

During the course of this project, we successfully fabricated an array capable of measuring intramural resistivity for several layers of the myocardium and developed a way to measure and quantify changes in resistivity to indicate intramural electrical uncoupling. Multi-level resistivity measurement is a novel concept in the realm of myocardial resistivity. Epicardial resistivity^{22,28,29,30,46} and mid-myocardial resistivity²⁶ have only been assessed in separate studies by different groups during myocardial ischemia. In ischemia preparations, resistivity is largely measured in the quiescent heart^{Jain} or in hearts paced at rates equivalent to SR.^{30,31,32} Assessment of resistivity during the rapid and irregular rhythms of VF certainly presented a challenge. Smith et al. cited the occurrence of VF during resistivity measurement in pigs;²⁶ however, data was excluded from experiments in which VF occurred within 2 minutes of ischemia and resistivity measurements were placed on hold to defibrillate VF occurring between 12-25 minutes of ischemia. While they do measure during VF in 4 of 9 experiments, they do not state any methods to account for these changes. To assess resistivity from data obtained in this study, a 40Hz filter was incorporated to remove low frequency activation components, voltage responses which were critically affected from overlap with activations were systematically excluded, and samples were taken 10s for each minute of VF to ensure an adequate number of quality pulses were obtained.

It was necessary to develop a definition for the onset of the steep rise in resistivity due to the fact that there is no standard definition. Ischemia studies have shown that cardiac resistivity changes in a characteristic manner producing an immediate first rise related to the onset of ischemia and reduction in perfusion pressure³⁸ or extracellular

space, a subsequent slow rise²² or plateau phase²⁶ related to a rise in extracellular resistance, and then a secondary, steep rise in resistivity related to the onset of increases in intracellular resistivity and thus electrical uncoupling.³⁸ The definition of electrical uncoupling onset, derived from resistivity values, has been described as the transition point from the slow rise in resistivity to the marked secondary rise,²² the time when resistivity shows an initial 3% increase from the minute prior,²⁸ the first point that demonstrates 10% rise in resistivity over best fit line through plateau phase,²⁶ or the change in the first derivative of resistivity with respect to time.²⁷ Resistivity data obtained during VF in the *in vivo* rabbit heart in this study did not fit the typical profile of ischemia. Qualitatively, resistivity profiles from the Endo, Mid, and Epi consisted of only a single prominent rise in most cases. Definitions based on identification of a steep, second rise (occurring after a small primary rise) which commonly develops during ischemia could not be applied to the VF resistivity data. Based on the definition described by Jain et al., observation of resistivity profiles obtained in previous studies of cardiac ischemia, and analysis of the relationship between resistivity and ARG data obtained in this study, a specific definition for the steep rise in resistivity was generated. Our definition was a more stringent criteria for the steep rise in that it not only required a larger resistivity increase than that described by Jain et al., it also required the occurrence of a subsequent continued increase. Resistivity measurements obtained during VF often contained small fluctuations in value from one minute to the next due to the nature of resolving response magnitudes amid underlying activations contained within the electrogram. The influence of the fluctuations were minimized by defining a substantial increase in resistivity as 5% and ensuring that the increase was not an outlier by requiring

the observance of continued increase (assessed as the average of the subsequent 3 values having a value 3% greater than the selected point).

The onset of electrical uncoupling during global ischemia^{22,28,46} occurs within 15.3-22.1min at a resistivity approximately 1.3-1.4 times baseline resistivity. Electrical uncoupling in regional ischemia^{26,27,29,30} occurs within 13-34min at a resistivity value ranging 1.4-2.0 times baseline resistivity. We found that resistivity during global ischemia rises in a manner similar to that previously reported with a small, initial rise immediately after onset of ischemia followed later by a very steep rise in resistivity which has been defined as the onset of electrical uncoupling.^{22,38} Mid electrical uncoupling (identified by onset of the steep rise in relative resistivity) during global ischemia occurs with a time course similar to uncoupling times of the regional ischemia range. Endo electrical uncoupling occurred at a time later than that reported in studies of global or regional ischemia. We found that electrical uncoupling developed with differential transmural time course where the Endo uncoupled latest. Since no studies have reported measurement of resistivity on the Endo, it follows that our assessment of the Endo uncoupling time is later than that previously reported. Average relative resistivity at the time of uncoupling for Endo and Mid are comparable to resistivity increases previously observed in regional ischemia studies and slightly larger than that reported for global ischemia. The results obtained in global ischemia studies demonstrate that the resistivity measurement system, analysis methods, and definition for the steep rise in resistivity can determine the onset of electrical uncoupling comparable to findings obtained by other investigators.

To our knowledge, this is the first study to compare the time course of resistivity changes during LDVF with that of global ischemia. The time course of the onset of steep increases in resistivity in the Endo, Mid and Epi during VF was much earlier compared to regional or global ischemia reported in this and other studies.^{22,26,27,28,29,30,46} The steep increases in resistivity found in LDVF were assessed with the same definitions and methods as in our global ischemia studies; therefore, indicating that electrical uncoupling occurs with early time course much earlier than in ischemia. VF may accelerate the electrophysiological changes which occur with ischemia. Persistent, rapid activations utilizing energy and metabolite stores may accelerate electrophysiological changes which occur in ischemia, causing early increases in gap junctional resistance, and thus resulting in early electrical uncoupling. Values of relative resistivity at the time of onset of the steep rise in resistivity were less than those shown in regional or global ischemia. While the criteria for the onset of the steep resistivity rise (electrical uncoupling) were the same for our VF and global ischemia studies, substantial increases in resistivity were achieved much earlier in time such that the value of relative resistivity at earlier time points were less than that of the later uncoupling times in ischemia.

A novel finding of this study is the transmural progression of the onset of steep resistivity rise reflecting electrical uncoupling in both LDVF and global ischemia. Through investigating resistivity in the Endo, Mid, and Epi during LDVF, it was revealed that the Epi steep rise developed earliest, with Mid and then Endo steep rises occurring subsequently. Furthermore, investigation of electrical uncoupling in the Endo and Mid during global ischemia revealed a similar transmural progression of electrical uncoupling from Mid to Endo. Our finding of transmural development of the steep resistivity rises in

VF, suggesting transmural electrical uncoupling, which occurs with similar time course as the development of the activation rate gradient supports our hypothesis that differential electrical uncoupling is the mechanism responsible for the VF activation rate gradient. These results further implicate heterogeneous expression and/or dephosphorylation of Cx43 as the biochemical mechanism by which electrical uncoupling operates.

Alternate Mechanisms for the Activation Rate Gradient

Several factors likely affect the electrophysiological changes which occur during long-duration ventricular fibrillation. Fibrillation induced ischemia may result in increased intracellular concentration of Ca^{2+} ,⁴⁷ intracellular acidosis,⁴⁸ reduction of ATP content,⁴⁹ and accumulation of amphipathic lipid metabolites⁵⁰ which affect gap junctional resistance. Differential transmural ion channel expression may affect excitability or refractoriness. A possible mechanism for the gradient could be differences in transient outward K^+ current. The transient outward K^+ current is much more significant in canine epicardium compared to the endocardium.⁵¹ However, evidence refuting this mechanism and supporting dispersion of I_{Na} inactivation properties have been reported. Corderio et al. found that in the presence of an I_{to} blocker, differences in canine Endo and Epi action potential morphology persisted and was attributed to lesser availability of I_{Na} in Epi cells due to a more negative half-inactivation voltage compared to Endo cells.⁵² Another mechanism for the rate gradient could be the differential Endo-Epi properties of ATP-regulated K^+ channels (K_{ATP}). K_{ATP} located in the Epi have greater sensitivity to reduction in intracellular ATP compared to channels in the Endo.⁵³ Theoretically, increased outward K^+ current would accelerate repolarization and prolong

postrepolarization refractoriness. Increased concentration of extracellular K^+ in normal, perfused, isolated rabbits hearts reproduced reduction of the LV epicardial VF activation rate which occurred during ischemic conditions, action potential duration was shortened, and activation threshold was increased.¹⁵ However, this increase in extracellular K^+ does not necessarily reflect the actions of K_{ATP} . Blockade of K_{ATP} by glybenclamide in normal, isolated dog hearts did not prevent the development of the Endo-Epi ARG, nor did it affect the time course of ARG development during LDVF.⁵⁴

Future Direction

Our study has demonstrated that the Endo to Epi gradient in activation rate coincides with electrical uncoupling which occurs transmurally beginning quickly after VF onset in the Epi. The Epi may have greater propensity for uncoupling due to lower expression of Cx43 in the Epi compared to deeper layers of the myocardium.⁴⁵ Or, dephosphorylation of Cx43 may progress more rapidly and with greater extent in the Epi compared to deeper myocardial layers during LDVF. In normal canine ventricles, the sub-epicardium has the fastest maximum action potential velocity, but smallest space constant and slowest conduction velocity. These finding suggest that transmural differences in coupling, rather than reduced excitability, contribute to conduction slowing.

Therefore, the next steps in the investigation of VF mechanisms will be to assess Cx43 as a biochemical basis for the development of the transmural electrical uncoupling. Dephosphorylation of Cx43 occurs during cardiac ischemia at the time when a steep, secondary rise in resistivity is observed.^{22,27,38} However, these ischemia studies did not

consider the possibility of transmural differences in resistivity or heterogeneous transmural Cx43 dephosphorylation. Our study suggests that cardiac conduction is reduced in a transmural fashion, likely due to heterogeneous changes in Cx43 phosphorylation. Investigation of Cx43 content and dephosphorylation during the course of LDVF with respect to intramural level may yield biochemical information on the mechanisms of uncoupling.

Limitations

The development of a novel intramural resistivity measurement system to determine transmural changes in resistivity suggesting electrical uncoupling has provided invaluable information on the mechanism of long-duration VF. However, this study did have limitations that should be considered and include long AC stimulation to induce VF, manual current switches for transmural current delivery, the use of anesthesia, and separate needles as a resistivity array. A major limitation of this study was the use of AC stimulation for 60s to induce VF. We suspect that VF may have initiated during the stimulation which led us to designate the time point when stimulation ceased and initial resistivity and mapping recordings were obtained as occurring at the first minute of VF. Neither ECG or electrograms could be evaluated while AC stimulation was delivered, therefore we were unable to determine the exact time of VF onset. It may be possible that a full 60s of VF did not occur prior to our first measurements. VF may have developed at any time within the range of 0 to 59s prior to the cessation of stimulation. By labeling initial measurements as occurring at 1 minute of VF, labeling onset time of steep resistivity rise at a time earlier than the true time with respect to VF onset could be

avoided. We could not confirm whether the onset of VF varied between experiments, but each experiment was treated identically. All hearts received stimulation for 60s, any VF occurring during stimulation was paced VF, and therefore VF did not freely progress until the cessation of stimulation. If VF occurred during stimulation, our steep resistivity rise onset times would actually have time labels later than the true onset time. Our findings of early steep resistivity rises indicating electrical uncoupling during VF is further solidified by the cautious time labeling used. Of the studies which electrically induce VF in rabbit, only a few specify VF induction duration, ranging between 2s and 20s.^{15,16,41,42} However, these studies were performed in isolated hearts. We found that LDVF in our *in vivo* rabbit model required a more aggressive induction protocol. Whether VF began during or after the stimulation, our results still show (1) the activation rate gradient develops soon into the VF episode, (2) the time of intramural resistivity increases correlate with changes in activation rate, and (3) differential transmural rise in resistivity occurs during LDVF. Therefore, this limitation does not have a major impact on the implications of this research.

A second limitation was the manual operation of current switches for transmural current delivery. During resistivity measurement, current was delivered through 3 to 4 levels of 4-needle linear arrays for each minute recorded. To achieve this, current output from one current source was connected to a switch box which then had connections to the different levels of electrodes designated for current delivery. Current was delivered for 10s in one intramural level, then turned off for 5s to allow time to switch current output to the next level. This was a limitation because it resulted in time differences of measurements between each layer. In every study, there was a 30s delay between

measurement of Endo and Epi resistivity. This was not a critical limitation because all resistivity values were measured in 1 minute intervals and evaluated relative to the value of resistivity at SR for the respective level. Therefore, any changes in resistivity were observed in equal intervals and relative to SR resistivity. It is possible that changes in resistivity could occur within 30s, however, since the concern of this study was general change in resistivity over time of VF this only means that transmural changes were observed within a maximum of 30s apart for each minute of VF. This could be resolved in future studies through the development and implementation of an automated switch box which could measure shorter intervals of resistivity with greater frequency or development of a system to measure resistivity in multiple tissue layers simultaneously.

A third limitation was the use of isoflurane as anesthesia during the surgical preparation, stabilization period, VF induction, and up to 30s of VF. Isoflurane invokes cardioprotection similar to ischemic preconditioning by limiting infarct size.^{55,56} The effects of isoflurane are suggested to be mediated by ATP-regulated K^+ channels, however, these studies did not yield information on whether the drug also inhibits electrical uncoupling. Studies which investigate ischemic preconditioning through the assessment of electrical uncoupling have found that preconditioning only delays the effects of ischemia.^{27,28} Therefore, the use of isoflurane in these studies may have reduced the extent to which electrical uncoupling occurred or possibly delayed the time course of uncoupling, however there is no direct evidence supporting this supposition.

A fourth limitation was the use of 4 separate plunge needles as a resistivity array. Care was taken to insert each needle transverse to the plane of the LV anterior surface at an approximate 90° angle. However, it is reasonable to acknowledge that there may have

been some slight differences in the directionality of each needle with respect to the array. This limitation was minimized by calculating resistivity relative to the value of resistivity obtained during baseline SR measurements for each intramural level in each study. In future studies, this limitation could be resolved by fabricating electrodes such that they are mounted and fixed on a non-conductive panel.

Conclusion

A disparity of knowledge regarding the mechanisms of LDVF prevents the development of improved therapeutic methods to treat SCA. Through the development of a novel preparation of LDVF in the *in vivo* rabbit heart and the originaive method to assess changes in resistivity transmurally, this study has investigated differential transmural electrical uncoupling as a mechanism for the ARG which develops during LDVF. Differential transmural steep rises in resistivity in the left ventricular myocardium progressed from the Epi toward the Endo. Onset of epicardial steep resistivity rise developed earliest during LDVF and was closely associated with the development of the Endo-Epi ARG. Steep rises in resistivity during LDVF presented much more quickly than during global myocardial ischemia. This new information on transmural resistivity changes suggests electrical uncoupling as the mechanism of LDVF and provides a platform for a targeted research approach to improve SCA therapy.

REFERENCES

1. Zheng ZJ, Croft JB, Giles WH, Mensah GA: Sudden Cardiac Death in the United States, 1989 to 1998. *Circulation* 2001;104:2158-2163.
2. Cummins RO: From concept to standard-of-care? Review of the clinical experience with automated external defibrillators. *Ann Emerg Med* 1989;18:1269-1275.
3. Campbell JP, Kroshus KS, Lindholm DJ, et al: Measuring the call-receipt-to-defibrillation interval: evaluation of prehospital methods. *Ann Emerg Med* 1995;26:697-701.
4. Weaver WD, Cobb LA, Hallstrom AP, Fahrenbruch C, Copass MK, Ray R: Factors Influencing Survival After Out-of-Hospital Cardiac Arrest. *J Am Coll Cardiol* 1986;7:752-757.
5. Chen PS, Wolf PD, Melnick SD, Danieley ND, Smith WM, Ideker RE: Comparison of Activation During Ventricular Fibrillation and Following Unsuccessful Defibrillation Shocks in Open-Chest Dogs. *Circ Res* 1990;66:1544-1560.
6. Choi BR, Nho W, Liu T, Salama G: Life span of ventricular fibrillation frequencies. *Circ Res* 2002;91:339-345.
7. Pogwizd SM, Corr PB: Mechanisms Underlying the Development of Ventricular Fibrillation During Early Myocardial Ischemia. *Circ Res* 1990;66:672-695.
8. Nanthakumar K, Huang J, Rogers JM, Johnson PL, Newton JC, Walcott GP, Justice RK, Rollins DL, Smith WM, Ideker RE: Regional Differences in Ventricular Fibrillation in the Open-Chest Porcine Left Ventricle. *Circ Res* 2002;91:733-740.
9. Zaitsev AV, Berenfeld O, Mironov SF, Jalife J, Pertsov AM: Distribution of Excitation Frequencies on the Epicardial and Endocardial Surfaces of Fibrillating Ventricular Wall of the Sheep Heart. *Circ Res* 2000;86:408-417.
10. Ideker RE, Klein GJ, Harrison L, Smith WM, Kasell J, Reimer KA, Wallace AG, Gallagher JJ: The transition to ventricular fibrillation induced by reperfusion after acute ischemia in the dog: a period of organized epicardial activation. *Circ* 1981;63:1371-1379.
11. Cha YM, Uchida T, Wolf PL, Peters BB, Fishbein MC, Karagueuzian HS, and Chen PS: Effects of chemical subendocardial ablation on activation rate gradient during ventricular fibrillation. *Am. J. Physiol.* 1995;269:H1998-H2009.

12. Venable PW, Taylor TG, Shibayama J, Warren M, Zaitsev AV: Complex structure of electrophysiological gradients emerging during long-duration ventricular fibrillation in the canine heart. *Am J Physiol* 2010;299:H1405-1418.
13. Worley SJ, Swain JL, Colavita PG, Smith WM, Ideker RE: Development of an Endocardial-Epicardial Gradient of Activation Rate During Electrically Induced Sustained Ventricular Fibrillation in Dogs. *Am J Cardiol* 1985;55:813-820.
14. Masse S, Farid T, Dorian P, Umapathy K, Nair K, Asta J, Ross H, Rao V, Sevaptsidis E, Nanthakumar K: Effect of global ischemia and reperfusion during ventricular fibrillation in myopathic human hearts. *Am J Physiol Heart Circ* 2009;297(6):H1984-H1991.
15. Caldwell J, Burton FL, Smith GL, Cobbe SM: Heterogeneity of Ventricular Fibrillation Dominant Frequency During Global Ischemia in Isolated Rabbit Hearts. *J Cardiovasc Electrophysiol* 2007;18:854-861.
16. Mandapati R, Asano Y, Baxter WT, Gray R, Davidenko J, Jalife J: Quantification of effects of global ischemia on dynamics of ventricular fibrillation in isolated rabbit heart. *Circulation* 1998;98:1688-1696.
17. Chorro FJ, Guerrero J, Canoves J, Martinez-Sober M, Mainar L, Sanchis J, Calpe J, Llavador E, Espi J, Lopez-Merino V: Quantification of the modifications in the dominant frequency of ventricular fibrillation under conditions of ischemia and reperfusion: An experimental study. *Pacing Clin Electrophysiol* 1998;21:1716-1723.
18. Wu TJ, Lin SF, Hsieh YC, Ting CT, Chen PS: Ventricular fibrillation during no-flow global ischemia in isolated rabbit hearts. *J Cardiovasc Electrophysiol* 2006;17:1-9.
19. Thomas SA, Schuessler RB, Berul CI, Beardslee MA, Beyer EC, Mendelsohn ME, Saffitz JE: Disparate effects of deficient expression of connexin43 on atrial and ventricular conduction. *Circulation* 1998;97:686-691.
20. Beyer EC, Goodenough DA, Paul DL: Connexin family of gap junction proteins. *J Membr Biol* 1990;116:187-194.
21. Kumar NM, Gilula NB: The gap junction communication channel. *Cell* 1996;84:381-388.
22. Beardslee MA, Kleber AG, Schuessler RB, Saffitz JE, et al: Dephosphorylation and intracellular redistribution of ventricular connexin43 during electrical uncoupling induced by ischemia. *Circ Res* 2000;87:656-662.
23. Ackmann JJ: Complex bioelectric impedance measurement system for the frequency range from 5Hz to 1MHz. *Annals of Biomedical Engineering* 1993;21:135-146.

24. Steendijk P, Mur G, Van der Velde ET, Baan J: The four-electrode resistivity technique in anisotropic media: theoretical analysis and application on myocardial tissue in vivo. *IEEE* 1993;40:1138-1148.
25. van Oosterom A, de Boer RW, van Dam RT: Intramural resistivity of cardiac tissue. *Med Biol Eng Comput* 1979;17:337-343.
26. Smith WT, Fleet WF, Johnson TA, Engle CL, Cascio WE: The 1B phase of ventricular arrhythmias in ischemic in situ porcine heart is related to changes in cell-to-cell electrical coupling. *Circulation* 1995;92:3051-3060.
27. Cinca J, Warren M, Carreno A, et al: Changes in myocardial electrical impedance induced by coronary artery occlusion in pigs with and without preconditioning. *Circulation* 1997;96:3079-3086.
28. Jain SK, Schuessler RB, Saffitz JE: Mechanisms of Delayed Electrical Uncoupling Induced by Ischemic Preconditioning. *Circ Res* 2003;92:1138-1144.
29. Padilla F, Garcia-Dorado D, Rodríguez-Sinovas A, Ruiz-Meana M, Inserte J, Soler-Soler J: Protection afforded by ischemic preconditioning is not mediated by effects on cell-to-cell electrical coupling during myocardial ischemia-reperfusion. *Am J Physiol Heart Circ Physiol* 2003;285:1909-1916.
30. Papp R, Gönczi M, Kovács M, Seprényi G, Végh Á: Gap junctional uncoupling plays a trigger role in the antiarrhythmic effects of ischaemic preconditioning. *Cardiovasc Res* 2007;74:396-405.
31. Tsai JZ, Will JA, Stelle SH, Cao H, Tungjitkusolmun S, Choy YB, Haemmerich D, Vorperian VR, Webster JG: In-Vivo Measurement of Swine Myocardial Resistivity. *IEEE Trans Biomed Eng* 2002;40:472-483
32. Cinca J, Warren M, Rodríguez-Sinovas A, Tresànceh M, Carreño A, Bragós R, Casas O, Domingo A, Soler-Soler J: Passive transmission of ischemic ST segment changes in low electrical resistance myocardial infarct scar in the pig. *Cardiovasc Res* 1998;40:103-112.
33. del Rio CL, McConnell PI, Kukielka M, Dzwonczyk R, Clymer BD, Howie MB, Billman GE: Electrotonic remodeling following myocardial infarction in dogs susceptible and resistant to sudden cardiac death. *J Appl Physiol* 2008;104:386-393.
34. Dossdall DJ, Tabereaux PB, Kim JJ, Walcott GP, Rogers, JM, Killingsworth CR, Huang J, Robertson PG, Smith WM, Ideker RE: Chemical ablation of the Purkinje system causes early termination and activation rate slowing of long-duration ventricular fibrillation in dogs. *Am J Physiol Heart Circ Physiol* 2008;295:H883-H889.

35. Huang J, Rogers JM, Killingsworth CR, Singh KP, Smith WM, Ideker RE: Evolution of activation patterns during long-duration ventricular fibrillation in dogs. *Am J Physiol Heart Circ Physiol* 2004;286:H1193-H1200.
36. del Rio CL, McConnell PI, Clymer BD, Dzwonczyk R, Michler RE, Billman GE, Howie MB: Early time course of myocardial electrical impedance during acute coronary artery occlusion in pigs, dogs, and humans. *J Appl Physiol* 2005;99:1576-1581.
37. Howie MB, Dzwonczyk R, McSweeney TD: An Evaluation of a New Two-Electrode Myocardial Electrical Impedance Monitor for Detecting Myocardial Ischemia. *Anesth Analg* 2001;92:12-18.
38. Kléber AG, Riegger CB, Janse MJ: Electrical Uncoupling and Increase of Extracellular Resistance After Induction of Ischemia in Isolated, Arterially Perfused Rabbit Papillary Muscle. *Circulation Research* 1987;61:271-279.
39. Garrey W: The nature of fibrillary contraction of the heart: its relation to tissue mass and form. *Am J Physiol.* 1914;33:397– 414.
40. Winfrey AT. Theory of spirals. In: Zipes DP, Jalife J, eds. *Cardiac Electrophysiology: From Cell to Bedside*. Philadelphia, Pa: WB Saunders; 1995:379 –389.
41. Pak HN, Oh YS, Liu YB, Wu TJ, Karagueuzian HS, Lin SF, Chen PS: Catheter Ablation of Ventricular Fibrillation in Rabbit Ventricles Treated With β -Blockers. *Circ* 2003;108:3149-3156.
42. Tang L, Hwang GS, Song J, Chen PS, Lin SF: Post-Shock Synchronized Pacing in Isolated Rabbit Left Ventricle: Evaluation of a Novel Defibrillation Strategy. *J Cardiovasc Electrophysiol* 2007;18:740-749.
43. Hillsley RE, Bollacker KD, Simpson EV, Rollins DL, Yarger MD, Wolf PD, Smith WM, Ideker RE: Alteration of Ventricular Fibrillation by Propranolol and Isoproterenol Detected by Epicardial Mapping with 506 Electrodes. *J Cardiovasc Electrophysiol* 1995;6:471-485.
44. Chen PS, Wolf PD, Dixon EG, Danieleley ND, Frazier DW, Smith WM, Ideker RE: Mechanism of ventricular vulnerability to single premature stimuli in open-chest dogs. *Circ Res* 1988;62:1191-1209.
45. Poelzing S, Akar FG, Baron E, Rosenbaum DS: Heterogeneous connexin43 expression produces electrophysiological heterogeneities across ventricular wall. *Am J Physiol Heart Circ Physiol* 2003;286:H2001-H2009.
46. Hund TJ, Lerner DL, Yamada KA, Schuessler RB, Saffitz JE: Protein kinase C ϵ mediates salutary effects on electrical coupling induced by ischemic preconditioning. *Heart Rhythm* 2007;4:1183-1193.

47. Dekker LR, Fiolet JW, Van Baval E, Coronel R, Opthof T, Spaan JA, Janse MJ: Intracellular Ca^{2+} , intercellular electrical coupling, and mechanical activity in ischemic rabbit papillary muscle: effects of preconditioning and metabolic blockade. *Circ Res* 1996;79:237–246.
48. White RL, Doeller JE, Verselis VK, Wittenberg BA: Gap junctional conductance between pairs of ventricular myocytes is modulated synergistically by H^+ and Ca^{++} . *J Gen Physiol* 1990;95:1061–1075.
49. Sugiura H, Toyama J, Tsuboi N, Kamiya K, Kodama I: ATP directly affects junctional conductance between paired ventricular myocytes isolated from guinea pig heart. *Circ Res* 1990;66:1095-1102.
50. Wu J, McHowat J, Saffitz JE, Yamada KA, Corr PB: Inhibition of gap junctional conductance by long-chain acylcarnitines and their preferential accumulation in junctional sarcolemma during hypoxia. *Circ Res*. 1993;72:879–889.
51. Litovsky SH, Antzelevitch C: Transient Outward Current Prominent in Canine Ventricular Epicardium but Not Endocardium. *Circ Res* 1988;62:116-126.
52. Cordeiro JM, Mazza M, Goodrow R, Ulahannan N, Antzelevitch C, Di Diego JM: Functionally distinct sodium channels in ventricular epicardial and endocardial cells contribute to a greater sensitivity of the epicardium to electrical depression. *Am J Physiol Heart Circ Physiol* 2008;295:H154–H162.
53. Furukawa T, Kimura S, Furukawa N, Bassett AL, Myerburg RJ: Role of cardiac ATP-regulated potassium channels in differential responses of endocardial and epicardial cells to ischemia. *Circ Res* 1991;68:1693–1702.
54. Taylor TG, Venable PW, Shibayama J, Warren M, Zaitsev AV: Role of K_{ATP} channel in electrical depression and asystole during long-duration ventricular fibrillation in ex vivo canine heart. *Am J Physiol Heart Circ Physiol* 2012;302:H2396-H2409.
55. Cason BA, Gamperl AK, Slocum RE, Hickey RF: Anesthetic-induced preconditioning: previous administration of isoflurane decreases myocardial infarct size in rabbits. *Anesthesiology* 1997;87:1182–1190.
56. Cope DK, Impastato WK, Cohen MV, Downey JM: Volatile Anesthetics Protect the Ischemic Rabbit Myocardium from Infarction. *Anesthesiology* 1997;86:699-709.

APPENDIX

IACUC Approval Form



THE UNIVERSITY OF ALABAMA AT BIRMINGHAM

Institutional Animal Care and Use Committee (IACUC)

NOTICE OF RENEWAL

DATE: January 3, 2013

TO: STEVEN POGWIZD, M.D.
VH -B140 0019
FAX: (205) 975-4720

FROM: 
Judith A. Kapp, Ph.D., Chair
Institutional Animal Care and Use Committee (IACUC)

SUBJECT: Title: Arrhythmia Mechanisms in Heart Failure
Sponsor: Internal
Animal Project Number: 130108356

As of January 28, 2013, the animal use proposed in the above referenced application is renewed. The University of Alabama at Birmingham Institutional Animal Care and Use Committee (IACUC) approves the use of the following species and numbers of animals:

Species	Use Category	Number in Category
Dogs	B	10
Mice	A	80
Mice	B	134
Rabbits	B	305

Animal use must be renewed by January 27, 2014. Approval from the IACUC must be obtained before implementing any changes or modifications in the approved animal use.

Please keep this record for your files, and forward the attached letter to the appropriate granting agency.

Refer to Animal Protocol Number (APN) 130108356 when ordering animals or in any correspondence with the IACUC or Animal Resources Program (ARP) offices regarding this study. If you have concerns or questions regarding this notice, please call the IACUC office at (205) 934-7692.

Institutional Animal Care and Use Committee
CH19 Suite 403
933 19th Street South
205.934.7692
FAX 205.934.1188

Mailing Address:
CH19 Suite 403
1530 3RD AVE S
BIRMINGHAM AL 35294-0019